Phytoplankton community structure and dynamics in the North Atlantic subtropical gyre

Carlos Cáceres[1,2], Antonella Rivera[1], Sonia González[1,3], Ricardo Anadón[1]

1 Área de Ecología. Departamento de Biología de Organismos y Sistemas de la Universidad de Oviedo, C/ Valentín Andrés Álvarez s/n. 33005, Oviedo, Asturias, España.

2 Department of Mathematics and Statistics. University of Strathclyde. Livingstone Tower, 26 Richmond St, Glasgow G1 1XH, Scotland, UK.

3 Centro Científico-Tecnológico Severo Ochoa, Universidad de Oviedo, C/ Dr. Fernando Bongera s/n. 33006, Oviedo, Asturias, España

Corresponding author: e-mail: carlos.l.caceres@gmail.com

Running head: Phytoplankton community structure and dynamics

Keywords: Phytoplankton growth rate, microzooplankton grazing rate, phytoplankton community structure, nutrient availability, subtropical gyres, dilution experiments, mixed models.

Abstract

Phytoplankton fuel epipelagic ecosystems and affect global biogeochemical cycles. Nevertheless, there is still a lack of quantitative information about the factors that determine both phytoplankton community structure and dynamics, particularly in subtropical gyres. Here, we estimated size fractionated phytoplankton growth (μ) and microzooplankton grazing rates (m) along a transect in the subtropical North Atlantic, from the island of Hispaniola to the Iberian Peninsula, by conducting dilution experiments and fitting mixed models. We also examined the relationship between nutrient availability and the differences in both phytoplankton community structure and size fractionated phytoplankton growth rates at two spatial scales (i.e. subtropical gyre and within-province spatial scale). Our results revealed high values for both phytoplankton growth and microzooplankton grazing rates. Phytoplankton growth (0.00 – 1.19 d^{-1}) displayed higher variability among stations, biogeochemical provinces and size fractions than the microzooplankton grazing rate (0.32 – 0.74 d^{-1}). Differences in phytoplankton community structure were associated with dissolved inorganic nitrogen (0.72- 5.85 µM; R^2= 0.19) and squared Brunt-Väisälä frequency (R^2= 0.21) at the whole gyre scale. Conversely, the differences in phytoplankton growth rate showed a weak relationship with those properties ($R^2 \leq 0.05$) at that scale, but a stronger relationship at the within province scale ($R^2 \geq 0.07$). These results support the idea that phytoplankton grow at high rates in oligotrophic subtropical gyres, this is likely due to the selection of phytoplankton groups with functional traits suited to exploit low nutrient availability. Thus, shedding new, multi-scale knowledge on the commonly misunderstood “ocean deserts”.

1. Introduction

Phytoplankton influence most components of epipelagic ecosystems (Reynolds 2001) and affect global biogeochemical cycles (Falkowski et al. 1998). Phytoplankton community structure and dynamics are mainly the result of the balance between growth and mortality. Phytoplankton growth at a community level is determined by resource availability. Nevertheless, phytoplankton growth rate at the community level may also be impacted by the functional traits, related to resource acquisition and growth, of the populations that compose said community, i.e. by the phytoplankton community composition. Despite being influenced by several factors, phytoplankton mortality is mainly driven by microzooplankton grazing (Calbet and Landry 2004). Microzooplankton grazing may also influence phytoplankton growth through nutrient regeneration, particularly in oligotrophic waters (Goldman 1984). To understand and predict phytoplankton community structure and dynamics and ecosystem functioning, the variability in phytoplankton growth and microzooplankton grazing must be disentangled. However, few studies discussed this question (e.g. Landry et al., 2009). In fact, to our knowledge, only the review of Calbet and Landry (2004) did it at a global scale. According to their results, differences among habitats were more pronounced in phytoplankton growth than in microzooplankton grazing rates.

The North Atlantic subtropical gyre mainly encompasses two biogeochemical provinces as defined by Longhurst (2007); the North Atlantic Tropical Gyral Province (NATR) and the North Atlantic Subtropical Gyral Province (NAST), which is divided in two sub-provinces (NAST-W and NAST-E). In those provinces, it is often believed that phytoplankton communities are characterized by low biomass, primary production and growth rates; and dominated by picoplankton. This is commonly attributed to the low

nutrient concentrations in the area (Marañón et al. 2000; Marañón 2005; Teira et al. 2005). However, the influence of nutrient availability on phytoplankton community structure and growth rate at different spatial scales (i.e., at a subtropical gyre or at a within-province spatial scale) has rarely been compared, despite the known importance of scale in ecological processes (see Levin 1992). Also, the influence of phytoplankton community composition, suited to exploit the low nutrient conditions, on the growth of the phytoplankton community might be misunderstood.

Here we used a novel approach to investigate the variability of phytoplankton growth rate (μ) and microzooplankton grazing rate (m) along with the relationship between nutrient availability and both the phytoplankton growth and community structure across the subtropical North Atlantic Ocean. First, we grouped the sampling stations into provinces and subprovinces defined by Longhurst (2007). Second, through dilution experiments (Landry and Hassett 1982) and mixed models we estimated phytoplankton growth and microzooplankton grazing rates for each province, size fraction and sampling station. To our knowledge, this is the first study where mixed models were employed to analyze data from dilution experiments. Third, we examined the relationship between phytoplankton community structure and phytoplankton growth and the effect of nutrient availability on both these variables. These analyses were carried out at the subtropical gyre spatial scale, which encompassed all sampled area, and at the within-province spatial scale. Our results showed that the variability of phytoplankton growth rate was higher than the variability of microzooplankton grazing rate. In addition, we found that nutrient availability only had a weak influence on the size-fractionated phytoplankton growth rates at the subtropical gyre spatial scale.

2. Methods

We sampled 16 stations along a SW-NE transect in the North Atlantic Ocean, between the SE of Hispaniola island of Hispaniola (S1, 67.48°W 19.26°N, March 24th) and the NW of the Iberian Peninsula (S16, 14.73°W 41.57°N, April 8th) as part of the *Buque Escuela Oceanográfica 2011* initiative (Fig. 1), within the framework of *Malaspina 2010 Expedition*. We performed 12 dilution experiments to estimate phytoplankton growth and microzooplankton grazing rates (Fig. 1) throughout the crossed biogeochemical provinces (NATR and NAST). The dilution experiments analyses were complemented with data on the physical, chemical and biological properties of the water column and satellite-derived altimetry and geostrophic velocities.

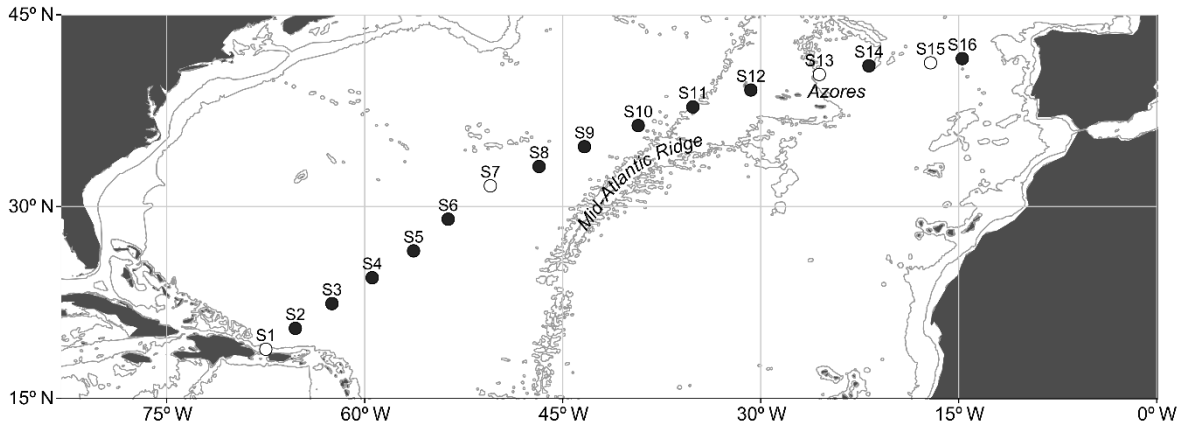

Fig. 1 Map showing the location of the 16 sampling stations (S1-S16) between Hispaniola and the Iberian Peninsula. Black dots indicate stations where dilution experiments were performed. White dots represent stations where experiments were not conducted.

2.1. Water column properties

Vertical distributions of temperature, salinity and fluorescence were obtained using a SBE-19 CTD equipped with a SeaPoint fluorometer mounted in a rosette equipped with 24, 12 L Niskin bottles. We estimated seawater potential density anomaly (σ_θ) from temperature, salinity and pressure. Subsequently, squared Brunt-Väisälä frequency (N^2)

was calculated using the *oce* R package (Kelley 2014). Nutrient concentrations (NO_3^-, NO_2^-, NH_4^+, PO_4^- and silicates) were measured for water samples at several depths (5, 25, 50, 75, 100, 125, 150, 175 and 200 m depth) using Niskin bottles. Two aliquots from each depth were collected in polystyrene tubes and preserved at -80°C until their analysis with a Skalar autoanalyzer using the methods described in Tréguer and Le Corre (1975).

2.2. **Remote sensing data**

Remotely sensed altimeter products and absolute geostrophic satellite data were obtained for the sampling period from Ssalto/Duacs and distributed by Aviso, with support from Cnes (http://www.aviso.oceanobs.com/duacs/). Gridded geostrophic velocity and sea level anomaly data were estimated by merging data from several altimeters using the methods developed by Le Traon et al. (1998). Using this information, we identified several processes that can alter the sea water properties and directly affect local phytoplankton communities.

2.3. Classification of the stations

We sampled across a large area with heterogeneous biogeochemical properties, which encompassed two biogeochemical provinces defined in Longhurst (2007); NATR and NAST (subdivided into NAST-W and NAST-E). Provinces are constrained to a range of latitudes and longitudes, but they do not have a clearly defined extension. We combined the geographic and biogeochemical criteria proposed by Longhurst (2007) with visual inspection of vertical profiles of sea water properties, satellite images of geostrophic velocities and multivariate analysis techniques to classify the stations in the above mentioned provinces.

We obtained a symmetric dissimilarity matrix for the stations using Manhattan distance with the following standardized sea water properties: fluorescence, salinity and potential temperature at 10 m depth, depth of the chlorophyll maximum, sum of the squared Brunt-Väisälä frequency in the upper 200 m and the depth of the maximum squared Brunt-Väisälä frequency. Subsequently, we performed a non-metric multidimensional scaling (NMDS) based on stress minimization by means of majorization (SMACOF) using the *Smacof* R package (de Leeuw 2009) in R computing software (R Core Team 2014). We fitted each covariate to the two dimensions of the ordination space using the *vegan* package (Oksanen et al. 2013). This showed which variables were associated with the differences between stations.

2.4. Sampling and Experimental set-up

Water samples were collected from the maximum potential phytoplankton growth rate depth between 3 and 11 h (local time) using 12 L Niskin bottles. The maximum potential phytoplankton growth rate depth in the subtropical North Atlantic has been found slightly above the DCM (Cáceres et al. 2013). When the DCM was not observed (stations from NAST), we sampled at a depth with a similar percentage of surface irradiance to minimize any bias that might occur due to differences in light. These depths were selected by the fluorescence profiles and were further corroborated through chlorophyll profiles, constructed using fluorescence profiles, following the methodology employed in Graziano et al. (1996) based in Morel (1987) (Table 1).

Table 1. Sampling time, depth, approximate percentage of surface irradiance at the sampling and nutrients at the different stations.

Station	Sampling time	Depth (m)	Surface irradiance (%)	DIN (µM)	Silicates (µM)
S2	6:50	80	15	0.84	2.29
S3	7:00	80	14	0.84	0.98
S4	6:40	80	13	0.72	0.95
S5	6:50	80	15	0.81	0.89
S6	6:20	70	13	1.13	0.82
S8	10:40	50	5	0.89	0.83
S9	8:20	40	8	1.98	1.06
S10	8:40	40	8	5.85	2.06
S11	8:30	40	7	2.04	1.02
S12	8:00	25	16	2.95	1.39
S14	11:10	30	8	4.22	1.23
S16	8:10	20	9	3.06	0.46

Water was transferred to 25 L polyethylene carboys, wrapped in black plastic to avoid light exposure, using silicone tubing fitted with 200 µm mesh to eliminate mesozooplankton. Water from one of the carboys was filtered through a 0.2 µm AcroPak 1000 capsule filter with a Supor membrane to obtain fully diluted water. The first liters filtered were discarded in every experiment and filter capsules were changed every six experiments. Next, polycarbonate containers of 2.3 L were gently filled with different proportions of filtered and unfiltered seawater. In this study, we used four dilution treatments with dilution factor (*f*) of 1 (undiluted water), 0.75, 0.5 and 0.25 with two replicates for each treatment. Additionally, we incubated two undiluted containers with added nutrients to check the potential effects of nutrients. Nutrient mixture added to nutrient enriched treatments resulted in a final concentration of 1 mM ammonium (NH_4Cl), 0.5 mM phosphate (H_3PO_4), 5 nM iron ($FeSO_4$) and 0.1 nM manganese ($MnSO_4$). We did not add nutrients to all the treatments due to potential negative effects on the plankton community (Landry and Hassett 1982; Lessard and Murrell 1998).

Therefore, there is a risk of underestimating the experimental phytoplankton growth rates as a consequence of poor nutrient regeneration in the most diluted treatments.

We used on-deck incubators with calibrated blue light filters to simulate in situ light conditions. They were covered with black plastic at night to protect the experiments from the ship´s lights. Incubators were kept at a homogenous temperature that closely resembled the in situ seawater temperature (± 0.1°C). Capsule filters, tubes and containers were soaked and rinsed in 10 % HCL-Milli Q water and rinsed with Milli-Q after every experiment. Just before each experiment, they were rinsed with the 0.2 µm filtered seawater. Carboys were rinsed with Milli Q water after every use and rinsed with seawater from the sampling depth before every experiment.

2.5. Chlorophyll *a,* flow cytometry and phytoplankton

Two 1000 mL samples of undiluted seawater were taken from the 25 L containers at the beginning of the experiment (t_0) to estimate chlorophyll *a* (Chl *a*) concentrations. Samples were sequentially filtered through 10 µm, 2 µm and 0.2 µm polycarbonate filters, which were arranged in line filter funnels. Then, filters were frozen and stored in the dark for 24 h. Chlorophyll *a* was extracted in 10 mL of 90 % acetone for 12-24 h and measured using Perkin Elmer LS55 fluorometer. Initial Chl *a* concentrations in the diluted treatments were estimated by multiplying the average undiluted initial Chl *a* concentrations by the dilution factor. We took 1000 mL samples from every container at the end of the experiment (t_f) and followed the same procedure to filter and measure Chl *a*. In this way, we obtained Chl *a* measurements in every container at t_0 and t_f.

The picophytoplankton community was analyzed by flow cytometry (FCM) to estimate growth and microzooplankton grazing rates based on abundance measurements. Samples (1.8 mL) were taken at t_0 and t_f from every container. They were preserved

with a 1 % paraformaldehyde plus 0.05 % glutaraldehyde solution and stored at -80^{0}C. Just before the analysis, we added a solution of 1 μm fluorescent latex beads to use them as standards. Analyses were conducted using a FACSCalibur flow cytometer (Becton, Dickinson and Company) equipped with a blue (488 nm) laser. Phytoplankton were grouped and enumerated according to the side-scattered light (SSC), an indicator of cell size, the orange fluorescence (FL2, 585 nm) and red fluorescence (FL3, > 650 nm) signals. Four groups were identified: *Prochlorococcus, Synechococcus,* small picoeukaryotes and large picoeukaryotes (Calvo-Díaz and Morán 2006). If the initial cell counts in dilution treatments were very low, we estimated initial cell abundances by multiplying cell concentrations in undiluted containers by the corresponding nominal dilution (see Supplementary material).

Nano- and microphytoplankton abundances were estimated from samples taken from the carboy at the beginning of the experiments (except at S11 and S14, in which samples were taken at t_f). They were preserved with the 10 % glacial acetic acid Lugol solution. Sample aliquots were maintained in the laboratory during 24 h using 25 mL Utermöhl chambers (Utermöhl 1958). The entire bottom area of the slide was examined and cells were determined up to genus or species level by using an inverted microscope. *Nitzschia spp.* at S16 was counted only in one strip and subsequently converted to cells mL^{-1} using the appropriate conversion factor due to their high abundances.

2.6. Phytoplankton growth and microzooplankton grazing rates

Exponential phytoplankton growth was assumed across the dilution treatments, resulting in apparent growth rate (r) equal to:

$$r = t^{-1} \ln(P_t \, P_0^{-1})$$

where t is the incubation time, P_0 is the initial phytoplankton biomass (Chl *a* biomass or cell abundance) and P_t is the biomass at the end of the incubation. Commonly, phytoplankton growth rate (μ) and microzooplankton grazing rate (m) are estimated with a linear regression analysis of r against dilution factor (f), where μ is the intercept and m is the slope (Landry and Hassett 1982). Here we estimate μ and m by fitting mixed models using the *lme4* R package (Bates et al. 2013). We included the dilution factor as a covariate, province and phytoplankton group (phytoplankton size fraction or flow cytometry group) as fixed factors and station as a random factor (see Supplementary material). This allowed us to simultaneously estimate μ and m for every phytoplankton group and station and mean μ and m for all phytoplankton groups and provinces. Additionally, the parameters are estimated taking into account the hierarchical organization of the data (Gelman and Hill 2007), which is not accounted for when conducting separate linear regressions for every experiment (the method commonly employed). In this way, all the information contained in the data set is considered when estimating the rates in the different experiments, and greater weight is given to experiments with less uncertainty. This provides more robust estimates, which are less influenced by extreme results or potential errors. Additionally, the correlation among stations from the same province, i.e. the non-independence of the data, is taken into account. For all those reasons, and considering our interest in estimating not only the rates (μ and m) for each experiment but also the mean rates for each province and group, we find mixed models a more appropriate method than averaging μ and m for every province and group from the parameters obtained by fitting a linear regression in each experiment. Furthermore, we performed model selection followed by model averaging, recommended when more than one model has substantial support, to obtain a more robust estimate of the parameters and a more stabilized inference (Burnham and

Anderson 2002) (see Supplementary material). This multimodel inference approach also enabled us to estimate the relative importance of each variable by adding the scaled AICc weights (see Supplementary material) of all the models within the 95 % confidence set of models where the variable of interest was included (Burnham and Anderson 2002). In our case, we obtained the relative importance of station, province and phytoplankton group as predictors for phytoplankton growth rate and microzooplankton grazing rate (i.e. interaction between predictors and dilution factor). Finally, to check the validity of our approach we compared the rates obtained by using mixed models and model averaging with the ones obtained by fitting separate linear regressions to each experiment.

2.7. Multivariate analyses of relations between nutrients, phytoplankton community structure and growth

Multivariate statistics were used to analyze differences among stations with regard to phytoplankton community taxonomic structure, phytoplankton community size structure and size fractionated phytoplankton growth rates at the depths of maximum phytoplankton activity. In addition, we related differences among stations in those properties with the nutrient availability at both the subtropical gyre and the within-province spatial scale.

To analyze phytoplankton taxonomic structure, we considered the abundances of 31 different genera (identified using optical microscope and FCM) and two non-taxonomic groups (small and large picoeukaryotes). These abundances were standardized by dividing each value by the range of abundances of the corresponding group, to counteract the higher contribution of the most abundant groups to the dissimilarities among stations (Quinn and Keough 2002). Those dissimilarities were estimated using

Bray-Curtis measure. Then, we performed NMDS using SMACOF. Subsequently, we conducted Permutational Multivariate Analysis of Variance [PERMANOVA, (Anderson 2001)] using the *vegan* package (Oksanen et al. 2013) to estimate the relationship (R^2) between the differences in taxonomic community structure among stations and the availability of nutrients using the following sea water properties: dissolved inorganic nitrogen (DIN, $NH_4^+ + NO_3^- + NO_2^-$), silicates and accumulated N^2 in the 100 m below the sampling depth, which indicates the strength of stratification and, consequently, was used as a proxy for nutrient inputs from deeper waters. DIN and silicate measurements were from the same depth as the phytoplankton samples or the closest depth for which nutrient samples were available. Phosphates were not included in the analysis because of their high correlation with DIN at those depths (r = 0.99). PERMANOVA was conducted without including and including province as a predictor, which removes the effects of province, in order to estimate the variances explained by the covariates at the subtropical gyre and at the within-province spatial scales, respectively. By including province as a predictor we also estimated the variance explained by province. In addition, we included the interaction between province and different covariates, which highlights the differences in magnitude or direction of the relationship among provinces. We conducted the same analyses with phytoplankton community size structure (using size fractionated Chl *a*) and size-fractionated growth rates (obtained from dilution experiments), although in these cases we employed Euclidean distances to generate the dissimilarity matrices.

Finally, we explored the relationship of community structure (taxonomic and size) with growth rate at the two scales considered in our research. For the subtropical gyre scale, we estimated the correlation between dissimilarity matrices. For the province scale, we fitted a linear mixed model that assessed the relationship between size-fractionated Chl

287 *a* and growth rate in each province. The model included μ as a dependent variable,
288 centered Chl *a* as a covariate, province as a fixed factor and size fraction as a random
289 factor (see Supplementary material for further details). Chl *a* concentrations were
290 centered by subtracting the mean Chl *a* value for each phytoplankton size fraction in
291 each province. This analysis allows us to consider the different size fractions
292 simultaneously. We fitted a similar model using the size-fractionated *m* as a dependent
293 variable. This analysis can help us disentangle the role of grazing in nutrient
294 regeneration and in the relaxation of phytoplankton competition for nutrients (Cooper
295 1973; Bergquist and Carpenter 1986).

3. Results

296 **3.1. Sea water properties and classification of the stations**

297 Visual inspection of vertical profiles and satellite images revealed general patterns in
298 the evolution of the sea water properties along the transect (Supplementary material
299 Figs. 1 and 2). This was further corroborated using the NMDS ordination of the sea-
300 water properties, which enabled us to classify the stations into their corresponding
301 provinces and sub-provinces. S2 to S6 have similar values on axis 1; we classified them
302 as stations from NATR (Supplementary material Fig. 3). S7 to S16 were classified as
303 NAST stations. The boundary between both NAST sub-provinces, NAST-W and
304 NAST-E, was located between S11 and S12, coinciding with the topography of the Mid
305 Atlantic Ridge (Fig. 1). For a further description see Supplementary material.

306 **3.2. Phytoplankton abundances and community structure**

307 Differences in the taxonomic structure of phytoplankton communities along the transect
308 corresponded with provinces defined by Longhurst (2007). Indeed, province explained a
309 large amount of the variance in community structure among stations (R^2= 0.43,

PERMANOVA), which might reflect the differences in nutrient availability (see below). NATR stations formed a well-defined group (Fig. 2A) characterized by low abundance of *Synechococcus*, small picoeukaryotes, large picoeukaryotes and diatoms (Fig. 2B). The abundance of most groups increased in the NAST-W stations, with the exception of dinoflagellates, which exhibited homogeneous abundances along the transect, and *Prochlorococcus* (although *Prochlorococcus* reached its maximum concentration in S11). Most NAST-E stations showed higher abundances of large picoeukaryotes and diatoms than the NAST-W stations (Fig. 2B), which led to their distinction in the NMDS analysis (Fig. 2A). Our results showed a diatom bloom in S16 dominated by *Nitzschia delicatissima*, with low abundances of *Prochlorococcus* and *Synechococcus* (Fig. 2B, Supplementary material Table 9). This differentiated the S16 community from the rest of the NAST-E stations. Hence, S16 was possibly located at the boundary between NAST-E sub-province and the North Atlantic Drift Province (NADR) (See Longhurst 2007).

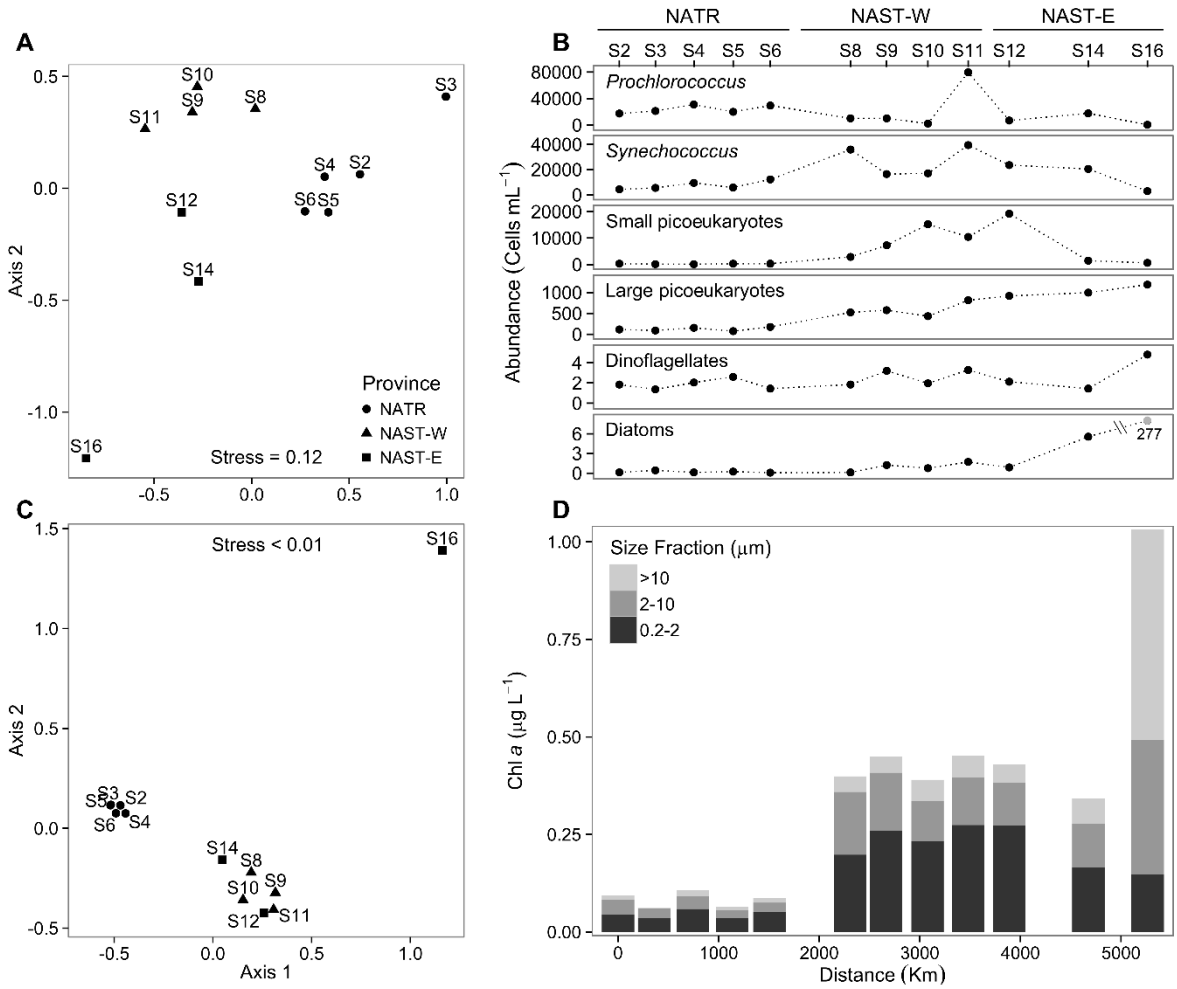

Fig. 2 Taxonomic composition and size structure of the phytoplankton community. (A) Two-dimensional configuration of stations obtained from the non-metric multidimensional scaling (NMDS) for phytoplankton community taxonomic structure. NMDS stress, a measure of the goodness of fit, is indicated. (B) Abundances of *Prochlorococcus*, *Synechococcus*, small picoeukaryotes, large picoeukaryotes, dinoflagellates and diatoms in the stations where dilution experiments were performed. Note the different scales of the abundances. Diatom abundance at S16 is out of the scale represented; its value is showed below the dot. (C) Two-dimensional configuration of stations obtained from the NMDS for phytoplankton size structure. (D) Size fractionated Chl *a* concentrations in the stations where dilution experiments were conducted.

Unsurprisingly, the phytoplankton community's size structure along the transect closely resembled the taxonomic structure of the community (Fig. 2C), with a correlation of r= 0.79 between dissimilarity matrices. Once again, province was a determining factor in explaining the variance (R^2= 0.53, PERMANOVA). NATR stations were clustered together (Fig. 2C) mainly due to their low Chl *a* concentrations in all three size fractions

(Fig. 2D). NAST stations were grouped close together, with the exception of S16. They shared high Chl *a* concentrations caused by the aforementioned increases in phytoplankton abundance. S16 appeared as an outlier in the NMDS plot due to high concentrations of Chl *a* in the medium and large phytoplankton size fractions.

3.3. Phytoplankton growth and microzooplankton grazing rates

3.3.1. Chl *a* analysis

Net growth rates derived from Chl *a* measurements were analyzed using different models to estimate phytoplankton growth and microzooplankton grazing rates. Phytoplankton growth rates ranged between 0.00 ± 0.39 d^{-1} and 1.19 ± 0.18 d^{-1} for the large phytoplankton size fraction in S16 and the medium size fraction in S6, respectively (Fig. 3; Supplementary material Fig. 4). The range of grazing rates was narrower, between 0.32 ± 0.25 d^{-1} at S16 and 0.74 ± 0.26 d^{-1} at S4. In fact, the variation of phytoplankton growth rate was higher than the variation of microzooplankton grazing rate among provinces (Fig. 4), size fractions within each province (Fig. 4), stations and among size fractions within each station (Fig. 3; Supplementary material Fig. 4; see below).

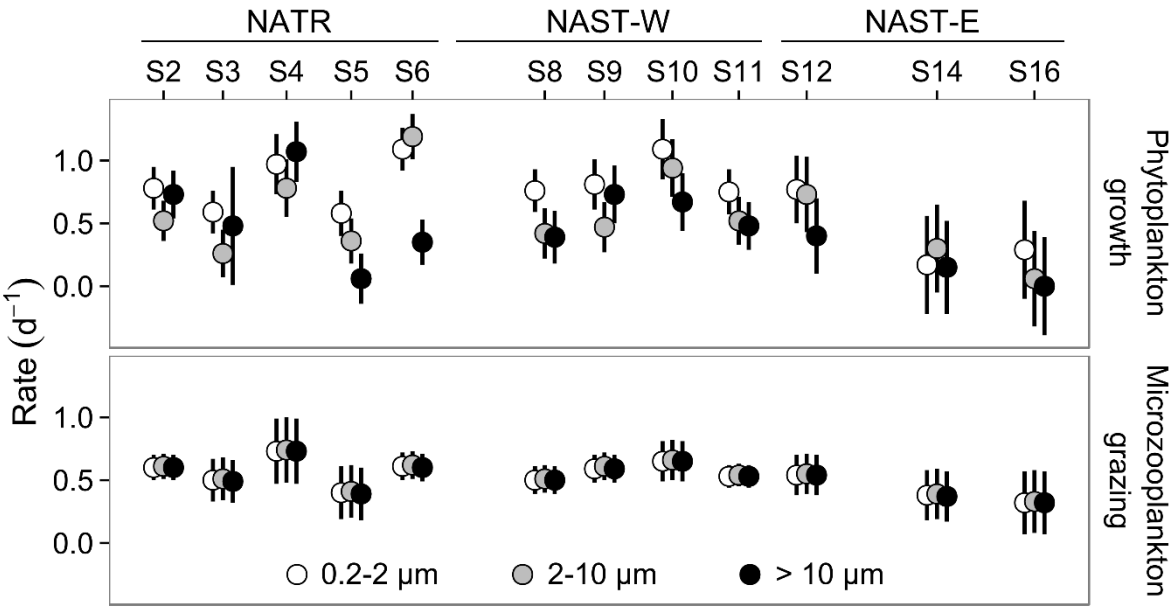

Fig. 3 Phytoplankton growth and microzooplankton grazing rates for each station and size fraction. Error bars represent 95% confidence intervals. Color indicates the phytoplankton size fraction. Geographical distance between stations has been kept.

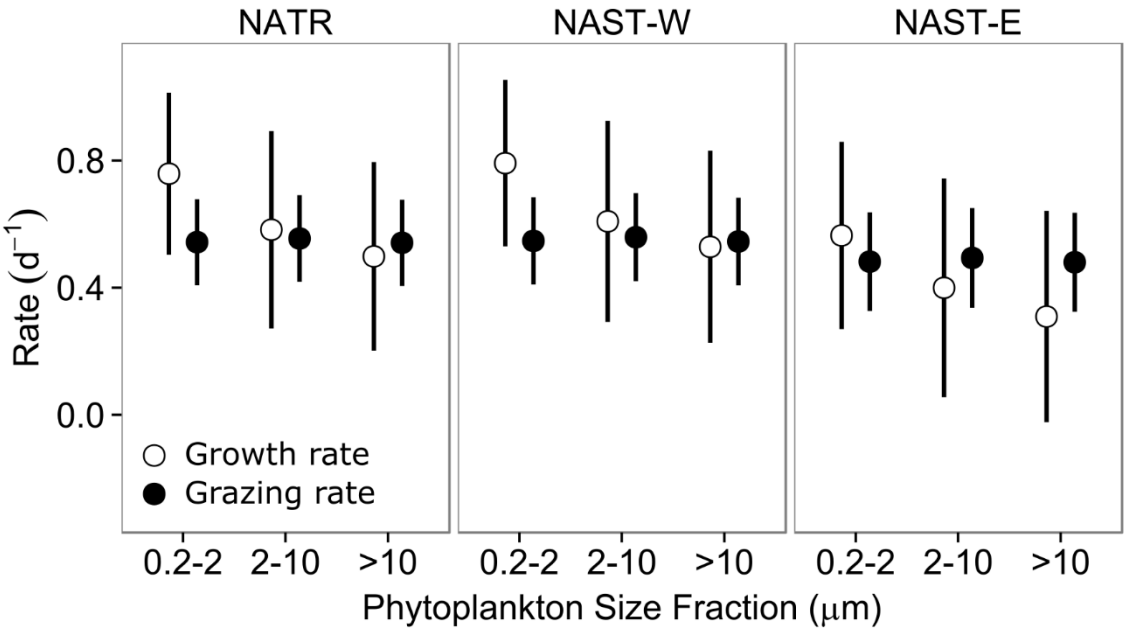

Fig. 4 Mean phytoplankton growth and microzooplankton grazing rates for each phytoplankton size fraction and province estimated from model averaging with models included in the 95% confidence set of models. Bars represent standard deviation.

Mean phytoplankton growth rates were similar in NATR and NAST-W and lower in NAST-E (Fig. 4). Mean grazing rates also decreased in NAST-E, but in a less

pronounced manner than mean growth rates (Fig. 4). Mean phytoplankton growth rates diminished with the phytoplankton size class (Fig. 4). Nevertheless, mean grazing rates were almost the same for all size fractions (Fig. 4). In summary, province affected both phytoplankton growth and microzooplankton grazing, although this effect is less pronounced in grazing rates. Conversely, size fraction only affects phytoplankton growth rate. These effects were confirmed by measurements of relative variable importance by using scaled AICc weights: the sum of scaled AICc weights of models that included province and the interaction between dilution factor and province (dilution x province) in the fixed structure was 0.57 and 0.33, respectively. Nevertheless, in the case of size fraction and the interaction between dilution factor and size fraction that sum was 0.99 and 0.13, respectively. Thus, the differences in mean phytoplankton net growth rates among provinces and especially among size fractions within each province were mainly determined by the differences in growth rates rather than by differences in microzooplankton grazing rates. The mentioned effect of province on the size fractionated phytoplankton growth rate was also revealed by the PERMANOVA analysis (R^2= 0.28. See also Fig. 5).

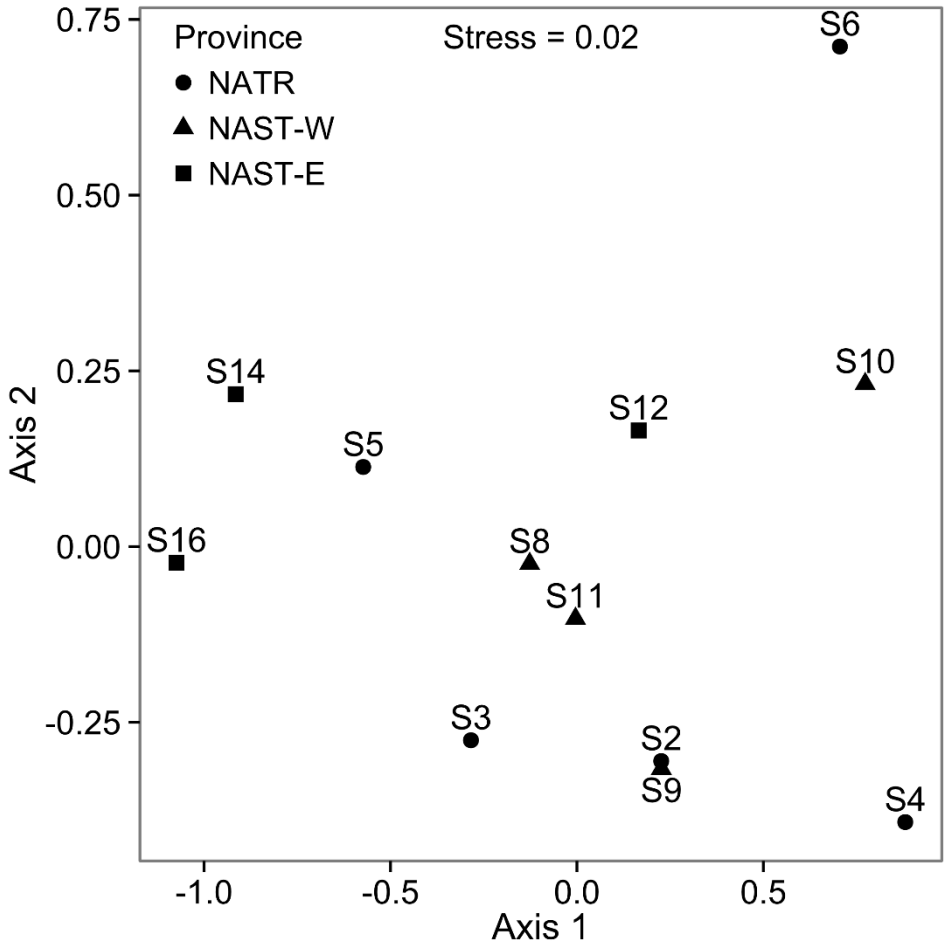

382

383 Fig. 5 Two-dimensional configuration of stations obtained from the non-metric
384 multidimensional scaling (NMDS) analysis conducted with size fractionated
385 phytoplankton growth rates. NMDS stress is also indicated.

386 The higher variability observed for phytoplankton growth rate than for
387 microzooplankton grazing rate among stations (Fig. 3, see standard deviations in Fig. 4)
388 and among size fractions within each station (Fig. 3) was also revealed by the sum of
389 scaled AICc weights. For models including a varying coefficient for the intercept
390 (growth) and the slope (grazing) the sum of scaled AICc weights were 1.00 and 0.65,
391 respectively. In these models, size fraction was included in the coefficient for the
392 intercept but not for the slope (Supplementary material Table 3). Again, differences in
393 phytoplankton net growth rates, both among stations and size fractions within each
394 station, would be mainly caused by differences in growth rates rather than by
395 differences in microzooplankton grazing rates. Province does not greatly affect the

variability (standard deviation) among stations of both rates (μ and m) (Fig. 4), in fact it was not included in the random structure of any of the models within the 95 % confidence set (Supplementary material Table 3).

3.3.2 Flow cytometry analysis

We estimated growth and microzooplankton grazing rates for picophytoplankton groups in the dilution experiments from FCM counts. As expected, the observed intercepts (phytoplankton growth rates) and slopes (microzooplankton grazing rates) were positive and negative, respectively, except in the case of cyanobacteria in NATR, where the contrary occurred (Supplementary material Fig.5). This effect on cyanobacteria has been previously reported in other dilution experiments, where it has been mainly attributed to the effect of trophic cascades (see Calbet and Saiz 2013 and references therein). The highest picophytoplankton growth and microzooplankton grazing rates were found in NAST-W and NAST-E sub-provinces, respectively (Fig. 6). Within NATR, growth and grazing rates were higher for picoeukaryotes than for cyanobacteria, whereas within NAST they were similar for the four picophytoplankton groups analyzed (Fig. 6). Additionally, in NAST-W picophytoplankton growth rate was higher than microzooplankton grazing rate; this difference was lower in the other provinces. Finally, we once again observed higher variations among stations in growth rates than in microzooplankton grazing rates (Fig. 6).

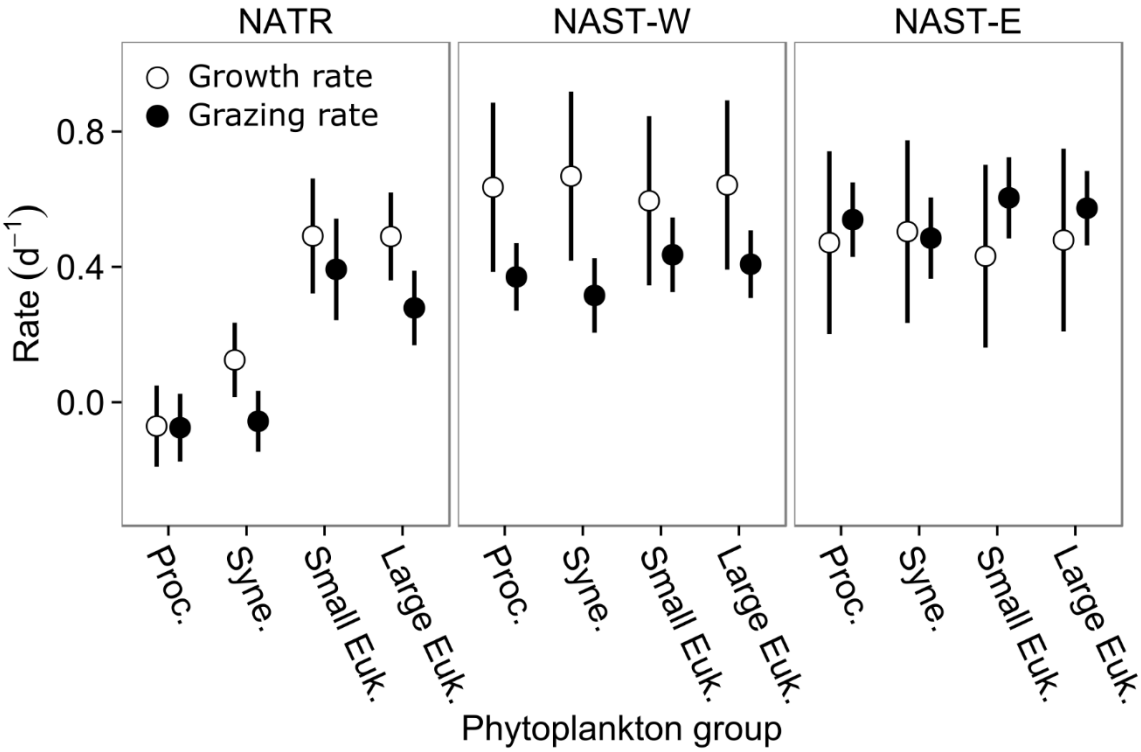

415

416 Fig. 6 Mean phytoplankton growth and microzooplankton grazing rates for each
417 picophytoplankton group and province estimated from model averaging with models
418 included in the 95% confidence set of models. Bars represent standard deviation.

419 We analyzed changes in FL3 and SSC signals between t_0 and t_f to detect potential
420 artifacts caused by dilution, diel growth cycles (some experiments lasted less than 24 h)
421 or photoacclimation processes that might affect Chl *a* and FCM estimates of growth and
422 grazing rates. We found no evidence of an effect of dilution treatment on relative FL3.
423 Nevertheless, we observed positively correlated increases in mean FL3 and SSC signals
424 of *Synechococcus* (estimated for each station) within the NATR province (r = 0.78, n =
425 5). Experiments in NATR lasted 21h and started when cells have just finished division
426 (Table 1); therefore FL3 and SSC signals showed values near the lowest trough of
427 *Synechococcus* light-dark growth cycle (Sweeney and Borgese 1989; Olson et al. 1990;
428 Jacquet et al. 1998). However, experiments ended when cells were still dividing and the
429 values of those signals were closer to the light-dark cycle peak. While we can not

discard the occurrence of photoacclimation processes, the estimates of *Synechococcus* growth rates from FCM counts could be underestimated.

3.3.3 Suitability of the method

In the case of the Chl *a* analysis, we compared the rates obtained by using mixed models and model averaging with those obtained by fitting separate linear regressions to each station and size fraction, the method traditionally employed (Supplementary material Fig. 4 and Table 7). Both approaches exhibited similar rates with only few exceptions. These exceptions occurred in experiments that showed a pattern far from norm, i.e. far from the rest of experiments, such as the 0.2-2 µm size fraction at S5, S6 and S8 or > 10 µm size fraction at S4 and S5 (Supplementary material Fig. 4 and Table 7). In those experiments, mixed models, by considering the entire data set and not only the data of the specific experiment, offered a more robust approach and a more stabilized inference, which was less influenced by extreme results or by potential errors occurred at specific experiments. Additionally, mixed models enabled the estimation of the rates for some factor levels without data (> 10 µm at S3) and improved the precision of the estimates in experiments with fewer observations (e.g. 2-10 µm at S3). In this way, the confidence intervals of the rates obtained by our approach were in general narrower than the ones obtained by fitting linear regressions (Supplementary material Table 7). The mean rates for each province and size fraction estimated from our approach and from averaging the rates obtained by fitting linear regressions to each experiment were in general similar too, although some differences were observed for both phytoplankton growth and microozooplankton grazing rate (Supplementary material Table 8), mainly in NAST-E.

It is worth emphasizing that the higher variability and differences observed for phytoplankton growth rate than for microzooplankton grazing rate among provinces, stations and size fractions were also observed when those rates were estimated by fitting linear regressions for every experiment (Supplementary material Table 8). Nevertheless, those variabilities were in general lower when they were estimated by following our approach, especially in the case of the microzooplankton grazing rate among size fractions within each station (Supplementary material Table 7).

3.4.Phytoplankton community properties and nutrient availability

The PERMANOVA analysis revealed an effect of DIN and cumulative N^2 on differences in taxonomic and size structure of phytoplankton community at the subtropical gyre spatial scale ($R^2 \geq 0.16$, Table 2). Explained variances were lower for silicate concentrations ($R^2 \leq 0.11$, Table 2). All those relationships were lower at the within-province spatial scale (after removing province effects) ($R^2 \leq 0.08$, Table 2). This means that differences in phytoplankton community structure are mainly driven by differences in nutrient concentrations and cumulative N^2 among provinces rather than within province. Nevertheless, the high variance explained by the interaction between province and silicate concentrations, together with the high abundance of diatoms and the low silicate concentrations observed in S16, suggested that silicate concentrations were strongly related with community structure in NAST-E. We repeated the analysis using relative standardized abundances of phytoplankton (standardized abundances divided by the sum of all the standardized abundances of each station), obtaining very similar results (data not shown).

Table 2. Variances explained (R^2) for the relationships between phytoplankton community properties and the different covariates obtained by the PERMANOVA analysis. Rows show the covariates for which the relationships were estimated. Columns show the different community properties analyzed. Sub-columns "Subtropical" and "Within-prov." pointed out the spatial scale at which relationships were estimated. Subtropical: the relationships were obtained considering the effects of the covariates at a subtropical gyre spatial scale. Within-prov: the relationships were estimated after removing the effects of province. Sub-column "Interaction" indicates the variance explained by the interaction between the covariates and province (it was not estimated for models including the three covariates because the number of parameters was too high).

Covariate	Phytoplankton community taxonomic structure			Phytoplankton community size structure			Phytoplankton community size fractionated growth		
	Subtropical	Within-prov	Interaction	Subtropical	Within-prov	Interaction	Subtropical	Within-prov	Interaction
DIN	0.19	0.04	0.09	0.16	0.01	0.07	0.02	0.07	0.19
Silicates	0.09	0.08	0.17	0.11	0.07	0.37	0.13	0.08	0.13
Cum. N2	0.21	0.05	0.10	0.24	0.00	0.02	0.05	0.10	0.11
DIN+Silicates+Cum.N2	0.47	0.24		0.52	0.20		0.32	0.34	

Contrary to phytoplankton community structure measurements, phytoplankton growth rates were not influenced by either DIN or cumulative N^2 at the subtropical gyre spatial scale ($R^2 \leq 0.05$, Table 2). Thus, differences in DIN and cumulative N^2 among provinces did not drive the differences in size fractionated phytoplankton growth rates. In fact, stations from NATR showed size fractionated phytoplankton growth rates similar to those observed at stations from NAST despite the general differences in DIN and cumulative N^2 between the two provinces (Table 1, Fig. 4, Supplementary material Fig.1). The relationship between the differences in phytoplankton growth rates and silicate concentration was stronger, although it was highly influenced by S16; the exclusion of S16 from the analysis reduced the explained variance from 0.13 to 0.05. Conversely, the relationship between differences in phytoplankton growth and both DIN and cumulative N^2 increased after removing the effects of the differences among provinces, indicating an effect of those covariates on phytoplankton dynamics at the within-province spatial scale, albeit a weak one ($R^2 \geq 0.07$, Table 2). Sure enough,

according to the explained variances for the interaction term, the relationship between the differences in phytoplankton growth and nutrient availability differed between provinces (Table 2). We obtained similar results when we repeated the analysis using phytoplankton growth rates estimated by fitting separate linear regressions for each station and size fraction (data not shown).

Differences in size fractionated phytoplankton growth rates were uncoupled from differences in phytoplankton community structure at the subtropical gyre spatial scale. We observed low correlations between the dissimilarity matrix of size fractionated phytoplankton growth rates and the dissimilarity matrices of both community taxonomic structure and size structure (r = 0.13 and r = 0.24, respectively). However, Chl *a* concentrations in all size fractions were positively correlated with the size fractionated growth and grazing rates within NATR (Fig. 7; Supplementary material Table 10). In contrast, the relationships were weaker, and in some cases negative, in both NAST sub-provinces (Fig. 7, Supplementary material Table 10).

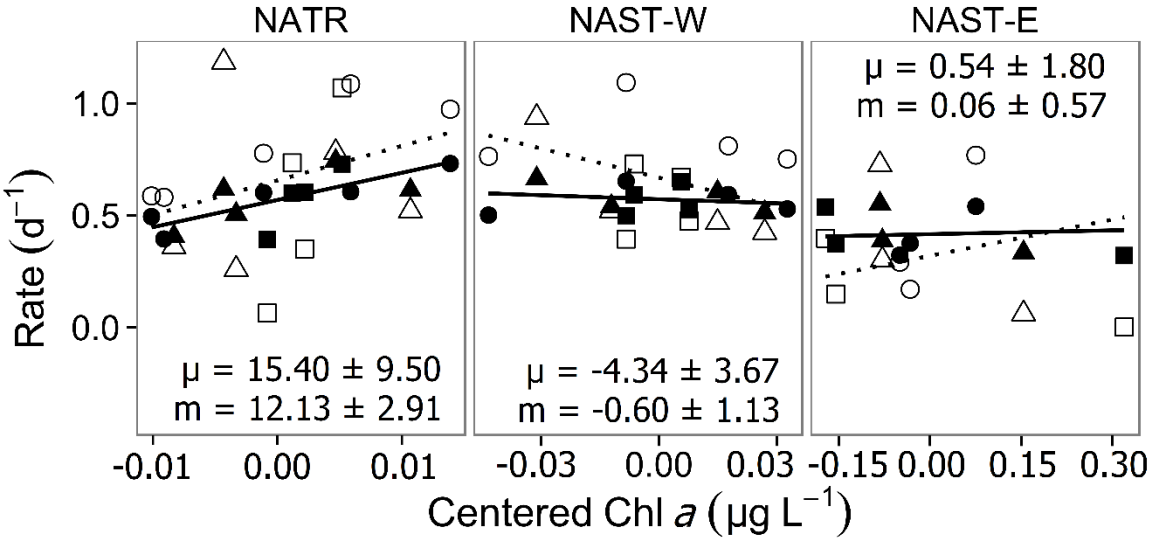

517

518 Fig. 7 Relationships between centered Chl *a* and both size fractionated phytoplankton
519 growth (μ) and microzooplankton grazing rates (m) in the different provinces. Note the
520 different scales of the x axes. White symbols indicate the phytoplankton growth rate and
521 black symbols the microzooplankton grazing rate. Shapes signify the phytoplankton size
522 fractions: 0.2-2 µm size fraction (circles), 2- 10 µm size fraction (triangles) and > 10
523 µm size fraction (squares). Lines indicate the linear fit for the relationships between μ
524 and centered Chl *a* (dotted) and m and centered Chl *a* (solid). μ is the slope (mean ±
525 standard error) of the relationship between phytoplankton growth rate and centered Chl
526 *a*. m is the slope (mean ± standard error) of the relationship between microzooplankton
527 grazing rate and centered Chl *a*.

4. Discussion

528 We estimated size fractionated phytoplankton growth and microzooplankton grazing
529 rates along a transect that covered a variety of conditions, which mirrored the
530 geographical partition of the North Atlantic proposed by Longhurst (2007). Our results
531 revealed that phytoplankton growth rate showed higher variability than
532 microzooplankton grazing rate among stations, provinces and size fractions.
533 Phytoplankton community structure differed across provinces and was associated with
534 nutrient availability at the subtropical gyre spatial scale. However, differences in
535 phytoplankton growth rate showed a weak relationship with nutrient availability at that
536 subtropical gyre spatial scale, being stronger at the within-province spatial scale.

Differences in phytoplankton growth rate and differences in community structure were only weakly correlated, although we observed a positive relationship between size-fractionated growth rate and size-fractionated Chl *a* within one of the provinces (NATR). Below, we discuss potential mechanisms for the observed variations in phytoplankton growth and microzooplankton grazing rates. Then, we discuss the relationship between nutrient availability, phytoplankton structure and phytoplankton dynamics at the two spatial scales considered.

4.1. Suitability of the statistical method

By fitting mixed models and conducting model averaging we took into account the hierarchical organization of the data and achieved a robust inference, estimating both specific rates for each station and size fraction and average rates for each province and size fraction. In general, the rates estimated by our approach were close to the ones obtained by fitting linear regressions for each experiment. The observed differences between both methodologies were mainly caused by the model selection based on AICc, which prevents overfitting by dealing with the trade-off between the goodness of fit and the complexity (number of parameters) of the model (Burnham and Anderson 2002), and the subsequent model averaging. Also, those differences arose due to the use of mixed models: when estimating the rates for a particular station and size fraction, mixed models take advantage of the information contained in other stations and size fractions. In addition, when estimating the average rates for each province and size fraction, mixed models assign a different weight to each experiment (depending on the information it contains). This does not occur when rates are estimated from the fitting of separate linear regressions for each experiment.

Our approach, both through using mixed models and model averaging, captured and unmasked the main patterns within the data without lead to overfitting. It enabled the detection of one of our major results, the higher variability in phytoplankton growth rate among provinces, stations and size fractions than in microzooplankton grazing rate, which could have been overlooked using traditional methods.

Based on our experience and the extensive literature on the use of mixed models (e.g. Gelman and Hill 2007), we encourage their application in future studies that aim to estimate mean rates in similar locations, depths or times, or studies focused on the variability of rates. Also, by conducting model selection and multimodel inference a more stable inference, i.e. more robust estimates of the rates, can be obtained. Furthermore, this procedure provides measurements on the importance of different predictors in explaining both the variability in phytoplankton growth and microzooplankton grazing rates (Burnham and Anderson 2002; Johnson and Omland 2004).

4.2. Phytoplankton growth and microzooplankton grazing rates

The variability in phytoplankton growth rate among provinces, stations and size fractions was higher than the variability in microzooplankton grazing rate. Greater differences among habitats for phytoplankton growth rate than for microzooplankton grazing rate were previously reported by Calbet and Landry (2004). Thus, differences in phytoplankton net growth rate among provinces, stations and size fractions were mainly determined by differences in the phytoplankton growth rate rather than by differences in the microzooplankton grazing rate. Microzooplankton grazing is considered one of the main drivers of phytoplankton mortality in subtropical oceans (Calbet and Landry 2004), this could entail that phytoplankton growth rate rather than mortality rate is

584 driving the differences in phytoplankton net growth rate among subtropical areas or
585 groups. Moreover, our present results on the high growth rates of the smallest size
586 fraction, coupled with information on the low sedimentation and mortality rate due to
587 mesozooplankton grazing found in the literature (Kiørboe 1993), would imply that the
588 relative contribution of the small size fraction to the total phytoplankton biomass was
589 increasing in most stations. Determining if in fact growth rate has a greater contribution
590 to the variability of the phytoplankton net growth rate than mortality rate will be a
591 crucial step in understanding phytoplankton dynamics, including phytoplankton blooms.
592 Future studies analyzing the variability of the growth and all the mortality sources of
593 phytoplankton (including viral lysis, mesozooplankton grazing and sedimentation in
594 addition to microzooplankton grazing) are required to confirm this hypothesis and
595 extrapolate it to other seasons or areas.

596 Phytoplankton growth rate tended to decrease as phytoplankton size increases in the
597 three provinces, in agreement with the studies that analyzed the relationship between
598 growth and size (Banse 1976; Tang 1995). The observed pattern could be due to a
599 decrease in the maximum phytoplankton growth rates as phytoplankton size increases
600 (Chisholm 1992; Edwards et al. 2012), although recent studies suggest that the highest
601 growth rates can be found in species of intermediate size (c. 100 μm^3, 5.76 µm spherical
602 diameter) (Marañón et al. 2013). Our results contrast with research carried out in
603 NAST-E in autumn or in other areas using the dilution technique, where large
604 phytoplankton grew as fast or faster than small phytoplankton (Olson and Strom 2002;
605 Calbet et al. 2008; Cáceres et al. 2013). In those cases, functional traits commonly more
606 developed in large phytoplankton and advantageous when nutrients are supplied in an
607 intermittent way, such as the maximum rate of nutrient uptake, the capacity to store

608 nutrients or the ability to perform vertical migration, would influence the growth of
609 phytoplankton populations (Reynolds 2006; Litchman et al. 2007).

610 According to our results, the microzooplankton grazing rate showed little differences
611 among size fractions. This result contrasts with previous research, which stated large
612 sizes provide phytoplankton protection against the predation by microzooplankton, thus
613 microzooplankton grazing rates are expected to be lower for the large phytoplankton
614 size fraction (Kiørboe 1993). Nevertheless, high grazing rates for the large
615 phytoplankton size fraction have been previously observed in the subtropical Northeast
616 Atlantic (Cáceres et al. 2013). The microzooplankton grazing rate depends on the ratio
617 between phytoplankton biomass grazed and phytoplankton biomass. Therefore, if this
618 ratio is constant across size fraction similar grazing rates are expected. In this way, the
619 functional and numerical responses of predators to the abundance of preys would
620 promote the association between phytoplankton biomass and phytoplankton biomass
621 grazed. The fact that zooplankton might prey on different size fractions of
622 phytoplankton, although with different efficiency (Hansen et al. 1994), could also
623 contribute to equalizing grazing rates among size fractions. On the contrary, the
624 specialization of grazers and the differences in their biology can lead to different
625 grazing rates on each phytoplankton size fraction, as it has been reported for other
626 seasons or places (Olson and Strom 2002; Calbet et al. 2008; Cáceres et al. 2013).

627

4.3. Nutrients and phytoplankton community structure and dynamics

The match between phytoplankton community structure, DIN and cumulative N^2 at the subtropical gyre scale could be caused by the selection of taxa with functional traits best suited to exploit the low nutrient concentrations in NATR (Litchman et al. 2007; Moore et al. 2008; Edwards et al. 2013). In fact, the abundance of *Prochlorococcus*, probably the most nutrient stress tolerant phytoplankton species (Reynolds 2006; Brun et al. 2015), was particularly high in NATR. That match is favored by the strong constraint that nutrient availability imposes on phytoplankton in subtropical areas (Reynolds 2001). Differences in taxonomic composition and functional traits of phytoplankton communities between biogeochemical provinces would lead to differences in growth-nutrient responses, promoting the weak relationship observed between phytoplankton growth and nutrients at a subtropical gyre scale. This situation was widely reported in studies focused on phytoplankton at a species level instead of community (e.g. Grover 1997); species with different functional traits may have similar growth rates under different nutrient concentrations and vice versa. Even populations of the same species may mitigate the effects of low nutrient concentrations due to phenotypic plasticity or genotype diversity and selection in traits affecting nutrient acquisition (Martiny et al. 2006; Van Mooy et al. 2009; Bonachela et al. 2011; Lomas et al. 2014; Biller et al. 2015). This would highlight the importance of functional diversity in maintaining and stabilizing phytoplankton growth at the subtropical gyre spatial scale, as it was previously determined by Díaz and Cabido (2001) for natural communities and ecosystem functioning. Thus, the growth rate of phytoplankton communities in oligotrophic subtropical gyres could be higher than the expected from the low nutrient concentrations (Cullen et al. 1992).

Other factors may contribute to the weak relationship between nutrient availability and phytoplankton growth at the subtropical gyre spatial scale, compensating for the low nutrient availability in NATR. Temperature stimulates chemical processes, metabolic reactions and phytoplankton growth (Eppley 1972; Raven and Geider 1988; Moore et al. 1995) and, as in other studies (Kamykowski and Zentara 1986), was negatively correlated with nutrients (Supplementary material Fig. 1). In addition, the large area encompassed by oligotrophic open ocean ecosystems like the NATR, together with the previous existence of stratified oceans (Falkowski and Oliver 2007), would favor the selection of species and ecotypes adapted to low nutrient concentrations. Furthermore, the stability of these areas could promote the match as well as the acclimation of phytoplankton communities to low nutrient concentration (see Venrick 1990). This match would be lower in areas with stronger seasonal cycles like NAST-E (see Longhurst 2007). Also, quick nutrient regeneration carried out by grazers and patches of high nutrient concentrations in these areas could increase nutrient availability for phytoplankton (Goldman 1984). Finally, differences in light conditions might also affect growth rate patterns and consequently their relationship with nutrients, although the careful selection of sampling depths would reduce that possibility.

Silicates displayed a stronger relationship with differences in phytoplankton growth rate at a subtropical gyre spatial scale than DIN and cumulative N^2. This relationship was mainly influenced by the diatom bloom in S16, which prompted the depletion of silicates. In fact, considering the low silicate concentrations and the notably higher than 1 N:Si ratio, a common N:Si ratio for diatoms (Brzezinski 1985), diatoms growth could be limited by Si in S16, as it was reported at higher latitudes (Turner et al. 1998; Longhurst 2007). This explains why phytoplankton growth rates of the medium and large size fraction in S16 were lower than in contiguous stations and those reported in

677 other studies (Calbet and Landry 2004; Marañón 2005). These particularities in the
678 biochemical properties of S16 could indicate that it was located in the frontier between
679 NAST-E and the North Atlantic Drift Province (NADR), where spring phytoplankton
680 blooms are more marked (Longhurst 2007). The diatom bloom could be responsible for
681 the lower grazing rates observed in S16; the increase in phytoplankton biomass would
682 have not been counterbalanced yet due to the lag in the zooplankton response. Similarly,
683 lower grazing rates associated to high phytoplankton biomasses have been previously
684 reported in other areas (Olson and Strom 2002).

685 The drivers for community structure differed among scales. Contrary to what was
686 observed at the subtropical gyre scale, DIN and cumulative N^2 had little influence on the
687 community structure at the within-province spatial scale, possibly caused by the fickle
688 nature of nutrient differences at this scale (Johnson et al. 2010). This would hinder the
689 match of the phytoplankton community structure to nutrient availability, or restrict that
690 match to very short time periods, making it difficult to detect. In fact, the high
691 concentration of DIN and silicates in S10, associated with the presence of a negative sea
692 level anomaly which entailed the ascent of enriched subsurface waters, did not cause
693 any marked increase in the abundance of any phytoplankton group. Nevertheless,
694 differences in phytoplankton community structure associated to fleeting nutrient inputs
695 have been reported for subtropical areas (McAndrew et al. 2007; McGillicuddy et al.
696 2007; Brown et al. 2008). That weak relationship between differences in community
697 structure and both DIN and cumulative N^2 at the within-province spatial scale would
698 imply that phytoplankton communities within each province would exhibit similar
699 functional traits associated with nutrient acquisition and growth. Thus, we would expect
700 a similar response to nutrients in these communities. This promoted the emergence of
701 the relationship observed between both DIN and cumulative N^2 and differences in size

fractionated phytoplankton growth at a within-province spatial scale, which does not occur at the larger subtropical gyre scale. In this way, phytoplankton growth rates estimated from both Chl *a* concentrations and FCM counts were high at S10, coinciding with the mentioned enhanced concentration of DIN and silicates. Studies in the subtropical North Atlantic relating phytoplankton growth and nutrients at a within-province scale are scarce, although increases in phytoplankton growth linked to nutrient inputs associated to mesoscale features has been suggested (McGillicuddy et al. 1998).

The uncoupling between phytoplankton community structure and growth at a subtropical gyre spatial scale, possibly favored by the response of those properties to nutrient availability, was reverted within the NATR province. The positive relationships observed between size fractionated μ and centered Chl *a* in NATR could be promoted by the also positive relationship found between size fractionated *m* and centered Chl *a*. Higher grazing rates when phytoplankton biomasses are higher entail higher nutrient regenerations (Bergquist and Carpenter 1986; Sterner 1986) and avoid increases in phytoplankton biomass that would lead to nutrient scarcity. The similar relationships with centered Chl *a* of both phytoplankton growth and microzooplankton grazing rates imply a coupling between growth and grazing, which has been previously reported in oligotrophic subtropical gyres (e.g. Quevedo and Anadón 2001) and argued to explain the high phytoplankton growth rates measured in those areas (Goldman 1984).

In conclusion, the relationships between nutrient availability and both the differences in phytoplankton community structure and growth were subject to change according to the scale at which they were analysed. Therefore, it is crucial to consider the spatial scale in the study of phytoplankton ecology (Levin 1992). Furthermore, the relationship between nutrient availability and phytoplankton growth rate is particularly complex. Here, we have observed the impact of scale and phytoplankton community structure on this

relationship. At the subtropical gyre spatial scale, we observed a weak relationship between the differences in phytoplankton growth and nutrient availability, which was promoted by the match between phytoplankton community structure and nutrient availability. This highlights the importance of taking into account the structure of biological communities when analysing their functioning and response to changes.

References

Anderson, M.J., 2001. A new method for non-parametric multivariate analysis of variance. Austral Ecol. 26, 32–46.

Banse, K., 1976. Rates of growth, respiration and photosynthesis of unicellular algae as related to cell size - a review. J. Phycol. 12, 135–140.

Bates, D., Maechler, M., Bolker, B., Walker, S., 2013. lme4: Linear mixed-effects models using Eigen and S4. R package version 1.0-5: http://CRAN.R-project.org/package=lme4.

Bergquist, A.M., Carpenter, S.R., 1986. Limnetic herbivory: effects on phytoplankton populations and primary production. Ecology 67, 1351–1360.

Biller, S.J., Berube, P.M., Lindell, D., Chisholm, S.W., 2015. *Prochlorococcus*: the structure and function of collective diversity. Nat. Rev. Microbiol. 13, 13–27.

Bonachela, J.A., Raghib, M., Levin, S.A., 2011. Dynamic model of flexible phytoplankton nutrient uptake. Proc. Nat. Acad. Sci. 108, 20633–20638.

Brown, S.L., Landry, M.R., Selph, K.E., Yang, E.J., Rii, Y.M., Bidigare, R.R., 2008. Diatoms in the desert: plankton community response to a mesoscale eddy in the subtropical North Pacific. Deep. Res. Part II 55, 1321–1333.

Brun, P., Vogt M., Payne M.R., Gruber N., O'Brien C.J., Buitenhuis E.T., Le Quéré C., Leblanc K., Luo Y-W., Ecological niches of open ocean phytoplankton taxa, Limnol. Oceanogr, 60, 2015, 1020–1038.

Brzezinski, M.A., 1985. The Si: C: N ratio of marine diatoms: Interespecific variability and the effect of some environmental variables. J. Phycol. 21, 347–357.

Burnham, K.P., Anderson, D.R., 2002. Model selection and multi-model inference: a practical information-theoretic approach. Springer.

Cáceres, C., Taboada, F.G., Höfer, J., Anadón, R., 2013. Phytoplankton growth and microzooplankton grazing in the subtropical Northeast Atlantic. PLoS One 8, e69159.

Calbet, A., Landry, M.R., 2004. Phytoplankton growth, microzooplankton grazing, and carbon cycling in marine systems. Limnol. Oceanogr. 49, 51–57.

Calbet, A., Saiz, E., 2013. Effects of trophic cascades in dilution grazing experiments:

761 from artificial saturated feeding responses to positive slopes. J. Plankton Res.
762 fbt067.

763 Calbet A., Trepat I., Almeda R., Saló V., Saiz E., Movilla J. I., Alcaraz M., Yebra L.
764 and Simó R., 2008. Impact of micro-and nanograzers on phytoplankton assessed by
765 standard and size-fractionated dilution grazing experiments. Aquat. Microb. Ecol.
766 50, 145–156.

767 Calvo-Díaz, A., Morán, X.A.G., 2006. Seasonal dynamics of picoplankton in shelf
768 waters of the southern Bay of Biscay. Aquat. Microb. Ecol. 42, 159–174.

769 Chisholm, S.W., 1992. Phytoplankton size, in: Falkowski, P.G., Woodhead, A.D.
770 (Eds.), Primary Productivity and Biogeochemical Cycles in the Sea. Plenum press,
771 pp. 213–237.

772 Cooper, D.C., 1973. Enhancement of net primary productivity by herbivore grazing in
773 aquatic laboratory microcosms. Limnol. Oceanogr. 18, 31–37.

774 Cullen, J.J., Yang, X., MacIntyre, H.L., 1992. Nutrient limitation of marine
775 photosynthesis, in: Falkowski, P.G., Woodhead, A.D. (Eds.), Primary Productivity
776 and Biogeochemical Cycles in the Sea. Plenum press, pp. 69–88.

777 de Leeuw J., M., P., 2009. Multidimensional scaling using majorization: SMACOF in
778 R. J. Stat. Softw. 31, 1–30.

779 Díaz, S., Cabido, M., 2001. Vive la différénce: plant functional diversity matters to
780 ecosystem processes. Trends Ecol. Evol. 16, 646–655.

781 Edwards, K.F., Litchman, E., Klausmeier, C.A., n.d. Functional traits explain
782 phytoplankton community structure and seasonal dynamics in a marine ecosystem.
783 Ecol. Lett. 16, 56–63.

784 Edwards, K.F., Thomas, M.K., Klausmeier, C.A., Litchman, E., 2012. Allometric
785 scaling and taxonomic variation in nutrient utilization traits and maximum growth
786 rate of phytoplankton. Limnol. Oceanogr. 57, 554–566.

787 Eppley, R.W., 1972. Temperature and phytoplankton growth in the sea. Fish. Bull. 70,
788 1063–1085.

789 Falkowski, P.G., Barber, R.T., Smetacek, V., 1998. Biogeochemical controls and
790 feedbacks on ocean primary production. Science. 281, 200–206.

791 Falkowski, P.G., Oliver, M.J., 2007. Mix and match: how climate selects
792 phytoplankton. Nat. Rev. Microbiol. 5, 813–819.

793 Gelman, A., Hill, J., 2007. Data analysis using regression and multilevel hierarchical
794 models. Cambridge University Press, Cambridge.

795 Goldman, J.C., 1984. Conceptual role for microaggregates in pelagic waters. Bull. Mar.
796 Sci. 35, 462–476.

797 Graziano, L.M., Geider, R.J., Li, W.K.W., Olaizola, M., 1996. Nitrogen limitation of
798 North Atlantic phytoplankton: analysis of physiological condition in nutrient
799 enrichment experiments. Aquat. Microb. Ecol. 11, 53–64.

800 Grover, J., 1997. Resource competition. Chapman & Hall, London.

801 Hansen, B., Bjørnsen, P.K., Hansen, P.J., 1994. The size ratio between planktonic
802 predators and their prey. Limnol. Oceanogr. 39, 395–403.

803 Jacquet, S., Lennon J.-F., Marie D. and Vaulot D., 1998. Picoplankton population
804 dynamics in coastal waters of the northwestern Mediterranean Sea. Limnol.
805 Oceanogr. 43, 1916–1931.

806 Johnson, J.B., Omland, K.S., 2004. Model selection in ecology and evolution. Trends
807 Ecol. Evol. 19, 101–108.

808 Johnson, K.S., Riser, S.C., Karl, D.M., 2010. Nitrate supply from deep to near-surface
809 waters of the North Pacific subtropical gyre. Nature 465, 1062–1065.

810 Kamykowski, D., Zentara, S.-J., 1986. Predicting plant nutrient concentrations from
811 temperature and sigma-t in the upper kilometer of the world ocean. Deep Sea Res.
812 Part A 33, 89–105.

813 Kelley, D., 2014. oce: Analysis of Oceanographic data. R package version 0.9-14.
814 http://CRAN.R-project.org/package=oce.

815 Kiørboe, T., 1993. Turbulence, phytoplankton cell size, and the structure of pelagic food
816 webs. Adv. Mar. Biol. 29, 1–72.

817 Landry, M.R., Hassett, R.P., 1982. Estimating the grazing impact of marine micro-
818 zooplankton. Mar. Biol. 67, 283–288.

819 Landry, M.R., Ohman, M.D., Goericke, R., Stukel, M.R., Tsyrklevich, K., 2009.
820 Lagrangian studies of phytoplankton growth and grazing relationships in a coastal
821 upwelling ecosystem off Southern California. Prog. Oceanogr. 83, 208–216.

822 Le Traon, Y.P., Nadal, F., Ducet, N., 1998. An improved mapping method of
823 multisatellite altimeter data. Journal of Atmospheric and Oceanic Technology. J.
824 Atmos. Ocean. Technol. 15, 522–534.

825 Lessard, E.J., Murrell, M.C., 1998. Microzooplankton herbivory and phytoplankton
826 growth in the northwestern Sargasso Sea. Aquat. Microb. Ecol. 16, 173–188.

827 Levin, S.A., 1992. The problem of pattern and scale in ecology. Ecology 73, 1943–
828 1967.

829 Litchman, E., Klausmeier, C.A., Schofield, O.M., Falkowski, P.G., 2007. The role of
830 functional traits and trade-offs in structuring phytoplankton communities: scaling
831 from cellular to ecosystem level. Ecol. Lett. 10, 1170–1181.

832 Lomas, M.W., Bonachela, J.A., Levin, S.A., Martiny, A.C., 2014. Impact of ocean
833 phytoplankton diversity on phosphate uptake. Proc. Natl. Acad. Sci. 111, 17540–
834 17545.

835 Longhurst, A., 2007. Ecological geography of the sea. Academic Press.

836 Marañón, E., 2005. Phytoplankton growth rates in the Atlantic subtropical gyres.
837 Limnol. Oceanogr. 50, 299–310.

838 Marañón, E., Cermeño, P., López-Sandoval, D.C., Rodríguez-Ramos, T., Sobrino, C.,
839 Huete-Ortega, M., Blanco, J.M., Rodríguez, J., 2013. Unimodal size scaling of
840 phytoplankton growth and the size dependence of nutrient uptake and use. Ecol.
841 Lett. 16, 371–379.

842 Marañón, E., Holligan, P.M., Varela, M., Mouriño, B., Bale, A.J., 2000. Basin-scale
843 variability of phytoplankton biomass, production and growth in the Atlantic Ocean.
844 Deep Sea Res. Part I 47, 825–857.

845 Martiny, A.C., Coleman, M.L., Chisholm, S.W., 2006. Phosphate acquisition genes in
846 *Prochlorococcus* ecotypes: evidence for genome-wide adaptation. Proc. Natl.
847 Acad. Sci. 103, 12552–12557.

848 McAndrew, P.M., Björkman, K.M., Church, M.J., Morris, P.J., Jachowski, N., le B.
849 Williams, P.J., Karl, D.M., 2007. Metabolic response of oligotrophic plankton
850 communities to deep water nutrient enrichment. Mar. Ecol. Prog. Ser. 332, 63–75.

851 McGillicuddy Jr. D. J., Anderson, L.A., Bates, N.R., Bibby, T., Buesseler, K.O.,
852 Carlson, C.A., Davis, C.S., Ewart, C., Falkowski, P.G., Goldthwait, S.A., Hansell,
853 D.A., Jenkins, W.J., Johnson, R., Kosnyrev, V.K., Ledwell, J.R., Li, Q.P., Siegel,
854 D.A., Steinberg, D.K., 2007. Eddy/wind interactions stimulate extraordinary mid-
855 ocean plankton blooms. Science. 316, 1021–1026.

856 McGillicuddy, D.J.J., Robinson, A.R., Siegel, D.A., Jannasch, H.W., Johnson, R.,
857 Dickey, T.D., McNeil, J., Michaels, A.F., Knap, A.H., 1998. Influence of
858 mesoscale eddies on new production in the Sargasso Sea. Nature 394, 263–266.

859 Moore, C.M., Mills, M.M., Langlois, R., Milne, A., Achterberg, E.P., La Roche, Geider,
860 R.J., 2008. Relative influence of nitrogen and phosphorus availability on
861 phytoplankton physiology and productivity in the oligotrophic sub-tropical North
862 Atlantic Ocean. Limnol. Oceanogr. 53, 291–305.

863 Moore, L.R., Goericke, R., Chisholm, S.W., 1995. Comparative physiology of
864 *Synechococcus* and *Prochlorococcus*: influence of light and temperature on
865 growth, pigments, fluorescence and absorptive properties. Mar. Ecol. Prog. Ser.
866 116, 259–275.

867 Morel, F.M.M., 1987. Kinetics of nutrient uptake and growth in phytoplankton. J.
868 Phycol. 23, 137–150.

869 Oksanen, J., Blanchet, F.G., Kindt, R., Legendre, P., Minchin, P.R., O'Hara, R.B.,
870 Simpson, G.L., Solymos, P., Henry, M., Stevens, H., Wagner, H., 2013. vegan:
871 Community Ecology Package. R package version 2.2-10. http://CRAN.R-
872 project.org/package=vegan.

873 Olson, M.B., Strom, S.L., 2002. Phytoplankton growth, microzooplankton herbivory
874 and community structure in the southeast Bering Sea: insight into the formation
875 and temporal persistence of an *Emiliania huxleyi* bloom. Deep. Res. Part II 49,
876 5969–5990.

877 Olson, R.J., Chisholm, S.W., Zettler, E.R., Armbrust, E. V, 1990. Pigments, size, and
878 distribution of *Synechococcus* in the North Atlantic and Pacific Oceans. Limnol.
879 Oceanogr. 35, 45–58.

880 Quevedo, M., Anadón, R., 2001. Protist control of phytoplankton growth in the
881 subtropical North-East Atlantic. Mar. Ecol. Prog. Ser. 221, 29–38.

882 Quinn, G.P., Keough, M.J., 2002. Experimental design and data analysis for biologists.
883 Cambridge University Press.

884 R Core Team, 2014. R: A language and environment for statistical computing.

885 Raven, J.A., Geider, R.J., 1988. Temperature and algal growth. New Phytol. 110, 441–
886 461.

887 Reynolds, C.S., 2006. The ecology of phytoplankton. Cambridge University Press.

888 Reynolds, C.S., 2001. Emergence in pelagic communities. Sci. Mar. 65, 5–30.

889 Sterner, R.W., 1986. Herbivore´s direct and indirect effects on algal populations.
890 Science. 231, 605–607.

891 Sweeney, B.M., Borgese, M.B., 1989. A circadian rhythm in cell division in a
892 prokaryote, the cyanobacterium *Synechococcus* WH78031. J. Phycol. 25, 183–186.

893 Tang, E.P., 1995. The allometry of algal growth rates. J. Plankton Res. 17, 1325–1335.

894 Teira, E., Mouriño, B., Marañón, E., Pérez, V., Pazó, M.J., Serret, P., de Armas, D.,
895 Escánez, J., Malcolm, E., Woodward, S., Fernández, E., 2005. Variability of
896 chlorophyll and primary production in the Eastern North Atlantic Subtropical
897 Gyre: potential factors affecting phytoplankton activity. Deep Sea Res. Part I 52,
898 569–588.

899 Tréguer, P., Le Corre, P., 1975. Manuel d'analyse des sels nutritifs dans l'eau de mer
900 (utilisation de l'AutoAnalyzer Technicon). Université de Bretagne Occidentale.

901 Turner, R.E., Qureshi, N., Rabalais, N.N., Dortch, Q., Justić, D., Shaw, R.F., Cope, J.,
902 1998. Fluctuating silicate: nitrate ratios and coastal plankton food webs. Proc. Nat.
903 Acad. Sci. 95, 13048–13051.

904 Utermöhl, H., 1958. Zur vervollkommnung der quantitativen phytoplankton-methodik.
905 Mitt. int. Mitt. int. Ver. theor. angew. Limnol. 9, 1–38.

906 Van Mooy, B.A., Fredricks.H.F., Pedler, B.E., Dyhrman, S.T., Karl, D.M., Koblížek,
907 M., Lomas, M.W., Mincer, T.J., Moore, L.R., Moutin, T., Rappé, M.S., Webb,
908 E.A., 2009. Phytoplankton in the ocean use non-phosphorus lipids in response to
909 phosphorus scarcity. Nature 458, 69–72.

910 Venrick, E.L., 1990. Phytoplankton in an oligotrophic ocean: species structure and
911 interannual variability. Ecology 71, 1547–1563.

912

Acknowledgements

913 We thank the crew and scientist on board the R. V. Sarmiento de Gamboa in the BEO
914 cruise, especially J.M.F. Pajares and F. Echeverría. J.M.F. Pajares and M. Sendra
915 (Universidad de Cádiz) provided the data for the calibration of chlorophyll fluorescence.
916 We also thank the NASA Ocean Biology Processing Group at the Goddard Space flight
917 Center for providing and maintaining the MODIS data. The altimeter products were
918 produced by Ssalto/Duacs and distributed by Aviso with support from Cnes. We are

919 especially grateful to F.G. Taboada for his help with satellite data, mixed models and
920 comments on the manuscript. E. Litchman provided valuable advice and a revision,
921 which improved the quality of the manuscript. R. González-Gil made interesting
922 suggestions and helped with R software use. A.F. Pardiñas and A. Molina provided
923 information about multivariate statistics. This research was financed by the Ministry of
924 Science and Innovation of Spain (complementary action *CTM2009-08399-E/MAR*) and
925 the University of Cadiz (project *DIB06*). It was conducted within the framework of the
926 project Consolider-Ingenio Malaspina 2010 (CSD2008-00077). CC and AR were
927 supported by a FPU fellowship (ref. AP2008-03658 and AP2010-5376, respectively,
928 Spanish Ministry of Education).

Supplementary material

Material and methods

Phytoplankton growth and microzooplankton grazing rates.

We fitted mixed models to estimate phytoplankton growth (μ) and microzooplankton grazing rates (m). These were based on the linear regression model proposed by Landry and Hasset (1982), which estimates μ and m from phytoplankton apparent growth rate (r) and the dilution factor (f):

$$r = \mu + mf$$

This model would allow us to estimate μ and m for each phytoplankton group (phytoplankton size fraction or flow cytometry group) in each station by running it separately. However, we were also interested in estimating size fractionated μ and m for each province. Therefore, we included effects of province, phytoplankton group and station (as random factor) in the previous model, obtaining the following two global mixed models (note the different random structures):

$$r_{ijkl} = \mu_0 + \mu_{Prov} + \mu_{group} + \mu_{Prov.\,group} + \alpha_{station(Prov.)} + (m_0 + m_{Prov.} + m_{group} + m_{Prov.\,group} + \beta_{station(Prov.)})\, f + e_{ijkl}$$

$$r_{ijkl} = \mu_0 + \mu_{Prov.} + \mu_{group} + \mu_{Prov.\,group} + \alpha_{station,\,group} + (m_0 + m_{Prov.} + m_{group} + m_{Prov.group} + \beta_{station,\,group})\, f + e_{ijkl}$$

$$(\alpha_{station(Prov.)}\,,\ \beta_{station(Prov.)}) \sim N\,(0,\ \textstyle\sum_{station\ Prov.})$$

$$(\alpha_{station,\,group}\,,\ \beta_{station,\,group}) \sim N\,(0,\ \textstyle\sum_{station\ group})$$

$$e_{ijkl} \sim N\,(0,\ \sigma^2).$$

Where r_{ijkl} is the net growth rate when province = province$_i$, group = group$_j$, station= station$_k$ and dilution factor (f) = f_l. μ_0 is the intercept of the reference level. m_0 is the slope of the reference level. Province and group are fixed effects on both intercept ($\mu_{Prov.}$, μ_{group}) and slope ($m_{Prov.}$, m_{group}), whose interaction is also considered ($\mu_{Prov.\ group}$, $m_{Prov.\ group}$). Station is a random effect also acting on both intercept (α) and slope (β), being nested in province ($\alpha_{station(Prov.)}$, $\beta_{station(Prov.)}$) or interacting with phytoplankton group ($\alpha_{station,\ group}$, $\beta_{station,\ group}$) depending on the global model considered. This allowed the intercepts and slopes to vary between stations, estimating at the same time different variances for intercepts and slopes depending on the province or the phytoplankton group. Because of the relative low number of observations, we cannot include in the same model random structures considering province and group. Random coefficients follow a normal distribution with mean equal 0 and a variance which is estimated by model fitting. In the case of size fractionated Chl *a* data, $\sum_{station\ Prov.}$ and $\sum_{station\ group}$ are 6 x 6 symmetric covariance matrices containing each one 21 parameters: three intercept variances (one for each province or phytoplankton size fraction), three slope variances (one for each province or phytoplankton size fraction) and 15 covariances. The error term is represented by e_{ijkl}.

Mixed models nested in the two previous global models were fitted using the *lmer* function from the R package *lme4* (Bates et al. 2013). We fitted models containing the interaction between the covariate (dilution factor) and the two fixed factors considered (province or phytoplankton group) even when the main effects were not included in the model. Those models are equivalent to the hypothesis that grazing rate was affected by the analyzed factors whereas phytoplankton growth rate remained unaffected. We employed the second order Akaike information criterion (AICc) to perform model selection (see below), instead of AIC, because of the low ratio between sample size (n) and the number of estimated parameters (K) (Burnham and Anderson 2002).

From AICc we computed AICc weight (AICc w) for every model, a measurement of the strength of evidence of each model. In doing that, we used the R package *AICcmodavg* (Mazerolle 2013).

Model selection procedure was based on Zuur et al. (2009), but we performed model averaging to estimate μ and m from a 95 % confidence set of models, which may include several fixed and random structures, if the AICc w of the best model was < 0.9 (Burnham and Andersson 2002). We firstly determined the best random structures of the q random structures considered (Supplementary material Table 1) using the most complex fixed structure (see Zuur et al. 2009). Restricted maximum likelihood (REML) was used to fit the models because we compared random structures. We interpreted the AICc weights ($AICc\ w_{\ random\ str\ q|\ complex\ fixed\ str}$) as the probability of each random structure q being the best among the whole set of random structures considered. Instead of only selecting the best random structure, we obtained the 95 % confidence set of models by adding AICc weights from the highest to the lowest until the sum ($\sum$ AICc w) was ≥ 0.95 (Burnham and Anderson 2002). Then, we scaled the AICc weights of those models including the best random structures $q´$ to sum one ($scaled\ AICc\ w_{\ random\ str\ q´|\ complex\ fixed\ str}$). Subsequently, we took each random structure $q´$ and combined it with the different fixed structures p (Supplementary material Table 2). Because we were comparing models with different fixed structures but the same random structure, models were fitted using maximum likelihood (ML). We obtained the weight of selecting a model with fixed structure p given the random structure $q´$ ($AICc\ w\ fixed\ str_p|random\ str_{q´}$). This can be combined with the above estimate to yield the weight of the model associated to fixed structure p accounting for the uncertainty in the selection of the random structure $q´$ ($AICc\ w_{pq´}$).

$$AICc\ w_{pq´} = (AICc\ w_{fixed\ str\ p\ |\ random\ str\ q´}) (scaled\ AICc\ w_{\ random\ str_{q´}\ |\ complex\ fixed\ str})$$

Again, we obtained the 0.95 confidence set of models by summing AICc weights of models from the highest to the lowest until the sum was ≥ 0.95. Then, we scaled AICc weights to sum one.

Model averaging to estimate coefficients $\left(\tilde{\bar{\beta}}_j\right)$, i.e. the rates, was performed using the zero method proposed in Burnham and Anderson (2002):

$$\tilde{\bar{\beta}}_j = \sum_{i=1}^{R} model\ AICc\ w_i\ \widehat{\beta_{j,i}}$$

Where $\widehat{\beta_{j,i}}$ is the estimate of β_j for model i. If the predictor j was not included in the model $\widehat{\beta_{j,i}}$ was set to zero. This method entails the use of all R models included in the final set of models. The unconditional variances ($\widehat{\bar{Var}}$), which include both within and between model variation, were estimated using the equation 6.12 proposed by Burnham and Anderson (2002):

$$\widehat{\bar{Var}}\left(\tilde{\bar{\beta}}_j\right) = \sum_{i=1}^{R} model\ AICc\ w_i\ \left[\widehat{Var}\left(\widehat{\beta_{j,i}} \mid g_i\right) + \left(\widehat{\beta_{j,i}} - \tilde{\bar{\beta}}_j\right)^2\right]$$

We calculated unconditional standard error (se) as the square root of the unconditional variance estimator (Burnham and Anderson 2002). Unconditional 95 % CI was estimated multiplying unconditional standard error by two (Burnham and Anderson 2002).

In the case of flow cytometry data, we did not analyze all the experiments together because of the positive slopes commonly detected for *Prochlorococcus* and *Synechococcus* in NATR. If all the data were analyzed together, those unrealistic microzooplankton grazing rates would affect rates of the other groups, or the rates of *Prochlorococcus* and *Synechococcus* in the other two provinces, due to the analytical procedure of mixed models. Thus, we performed three separate analyses disaggregating the data in the following form: *Prochlorococcus* and *Synechococcus* in

NATR, large eukaryotes and small eukaryotes in NATR, and the four FCM groups together in NAST-W and NAST-E. We did not estimate relative importance of variables.

Flow cytometry analysis

Initial cell counts of some groups were very low in some experiments. When initial cell counts < 330 in the undiluted treatment, we estimated initial cell abundances in diluted containers multiplying cell concentrations in undiluted containers by the corresponding nominal dilution. This was the case of large eukaryotes in all the stations, small eukaryotes in NATR stations, S14 and S16, and *Prochlorococcus* in S16. Departures from the nominal dilution caused by inexact bottle fillings would be unaccounted for with this approach and could be a source of error in the estimated rates (Worden and Binder 2003). Nevertheless, we discarded this potential mistake by graphically checking that observed initial abundances of the more abundant groups (*Prochlorococcus* and *Synechococcus*) in diluted samples were similar to the abundances obtained multiplying observed abundances at the undiluted samples by the nominal dilutions (data not shown).

Relation between size fractionated Chl *a* and growth

We fitted the following mixed models to estimate the relationship between phytoplankton community size structure and size fractionated phytoplankton growth and grazing rates in each province and subprovince:

$$\mu_{ijk} \curlyvee m_{ijk} = a_0 + a_{Prov.} + \alpha_{size} + (b_0 + b_{Prov.} + \beta_{size})\, Chl\ a^* + e_{ijk}$$

$$(\alpha_{size}\ ,\ \beta_{size}) \sim \mathrm{N}\ (0,\ \textstyle\sum_{size})$$

$$e_{ijk} \sim \mathrm{N}\ (0,\ \sigma^2)$$

Where μ_{ijk} and m_{ijk} are phytoplankton growth and microzooplankton grazing rates, respectively, when province = $province_i$, size = size $fraction_j$, station = $station_k$, and *Chl a** = ($Chl\ a_{ijk}$ - $\overline{Chl\ a_{ij}}$). In this way, we estimated a general relationship for the three size fractions without considering differences in Chl *a* concentrations between size fractions, *i.e.* to isolate within group effects (e.g. van de Pol and Wright 2006). a_0 and b_0 are the intercept and the slope, respectively, for the reference level. Province is a fixed effect acting on both intercept ($a_{Prov.}$) and slope ($b_{Prov.}$). α_{size} and β_{size} are random effects of size fraction on intercept and slope, respectively. $\sum_{size}$ is a 2 x 2 symmetric covariance matrix containing 3 parameters: a variance for the intercept, a variance for the slope and a covariance between them. e_{ijk} is the error term.

Results

Sea water properties and classification of the stations

Potential temperature at 10 m depth, the depth of the chlorophyll maximum and the variability of the N:P ratio decreased toward Iberian Peninsula. In contrast, fluorescence at 10 m depth, DIN and N:Si ratio increased toward Iberian Peninsula (Supplementary material Fig. 1). The geographic and depth patterns of DIN mimic the ones of NO_3^-, which was much more variable than NO_2^- and NH_4^+ (data not shown). Singularities were observed along the transect. This is the case of potential temperature in S4; salinity, potential temperature and nutrients in S10; or potential temperature, fluorescence and nutrients in S16 (Supplementary material Fig. 1). Singularities in S4 and S10 could be promoted by the presence of sea level anomalies (Supplementary material Fig. 2A).

The NMDS ordination of the sea-water properties helped classify stations in the corresponding provinces and sub-provinces. The low NMDS stress, a measure of the goodness of fit, supported the obtained configuration (Supplementary material Fig. 3). S2 to S6 have similar values on the axis 1, mainly defined by the depth of the chlorophyll maximum and fluorescence and temperature at 10 m depth. We classified them as stations from NATR (Supplementary material Fig. 3). The S7 showed marked differences from the contiguous stations, because of its location at the boundary between NATR and NAST (Supplementary material Figs. 1 and 3). According to Longhurst (2007), the front between both provinces is defined by the position of the Subtropical convergence (STC), which in winter (near to our sampling time) matches the surface end of the 20°C isotherm. This is in agreement with the grouping of S7 with NAST-W stations (S7 surface T = 19.8° C). The division of the group of the S7 to S16 stations, corresponding to the separation of NAST province into NAST-W and NAST-E, was supported by the observed geostrophic velocities (Supplementary material Fig. 2B). The boundary between both sub-provinces was located between S11 and S12, coinciding with the topography of the Mid Atlantic Ridge (see Fig 1), which limits the entrance of water from the western Atlantic (Longhurst 2007).

Figures and tables

Table 1. Different random structures considered in models fitted to parameterize phytoplankton growth (μ) and microzooplankton grazing rates (m). An *I* letter means that intercept, i.e. phytoplankton growth, can change between stations. Consequently a standard deviation (sd) for μ is estimated. An *S* letter means that slope, i.e. grazing, may change between stations and standard deviation is estimated for m. If *I* or *S* appears in columns *Station x Prov.* or *Station x Group*, a standard deviations for μ or m, respectively, is estimated for each level of the fixed factor.

	Random effects		
Structure	Station	Station x Prov.	Station x Group
1			
2	I		
3		I	
4			I
5	S		
6		S	
7			S
8	I & S		
9		I & S	
10			I & S
11	S	I	
12	I	S	
13	S		I
14	I		S

Table 2. Different fixed structures included in models fitted to parameterize phytoplankton growth (μ) and microzooplankton grazing rates (m). A cross (x) in the *Dilution* column means that dilution factor, i.e. grazing, was included in the model. An *I* letter means that a different intercept, i.e. an effect on phytoplankton growth rate, was estimated for every level of the factor. An *S* letter means that a different slope, i.e. an effect on grazing rate, was estimated for each level of the factor.

	Fixed effects			
Structure	Dilution	Group	Prov.	Group x Prov.
1				
2	x			
3	x		I	
4	x		S	
5	x		I & S	
6	x	I		
7	x	S		
8	x	I & S		
9	x	I	I	
10	x	I	I & S	
11	x	I & S	I	
12	x	I	S	
13	x	S	I	
14	x	S	S	
15	x	I	I & S	
16	x	I & S	I	
17	x	I & S	I & S	
18	x	I	I	I
19	x	I	I & S	I
20	x	I & S	I	I
21	x	I & S	I & S	I
22	x	S	S	S
23	x	S	I & S	S
24	x	I & S	S	S
25	x	I & S	I & S	S
26	x	I & S	I & S	I & S
27			I	
28		I		
29		I	I	
30		I	I	I

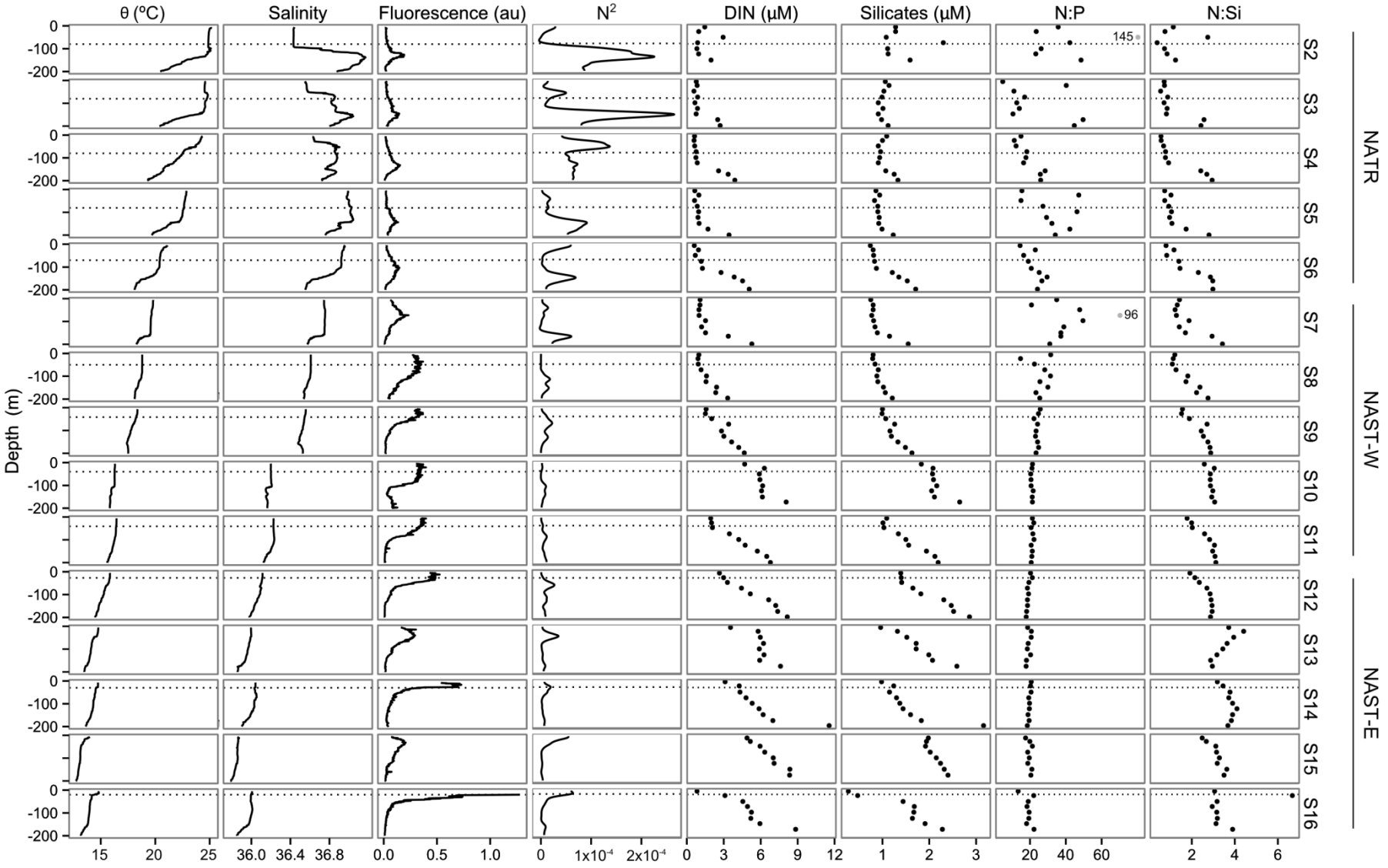
θ (ºC)
Salinity
Fluorescence (au)
N²
DIN (µM)
Silicates (µM)
N:P
N:Si
Depth (m)
0
-100
-200
145
96
S2
S3
S4
S5
S6
S7
S8
S9
S10
S11
S12
S13
S14
S15
S16
NATR
NAST-W
NAST-E
15
20
25
36.0
36.4
36.8
0.0
0.5
1.0
0
1x10⁻⁴
2x10⁻⁴
0
3
6
9
12
1
2
3
20
40
60
2
4
6

1087

Fig. 1 Vertical profiles of potential temperature (θ), salinity, fluorescence, square Brunt-Väisälä frequency (N^2), dissolved inorganic nitrogen (DIN), silicates, N:P ratio (N:P) and N:Si ratio (N:Si). Horizontal dotted lines indicate sampling depths of dilution experiments. Fluorescence values of S16 up to 20m depth were excluded in order to increase the resolution of the panels at lower fluorescence values. N^2 profiles were smoothed. Grey points in N:P ratio profiles at S2 and S7 show values out of the scale, their values are indicated close to the points

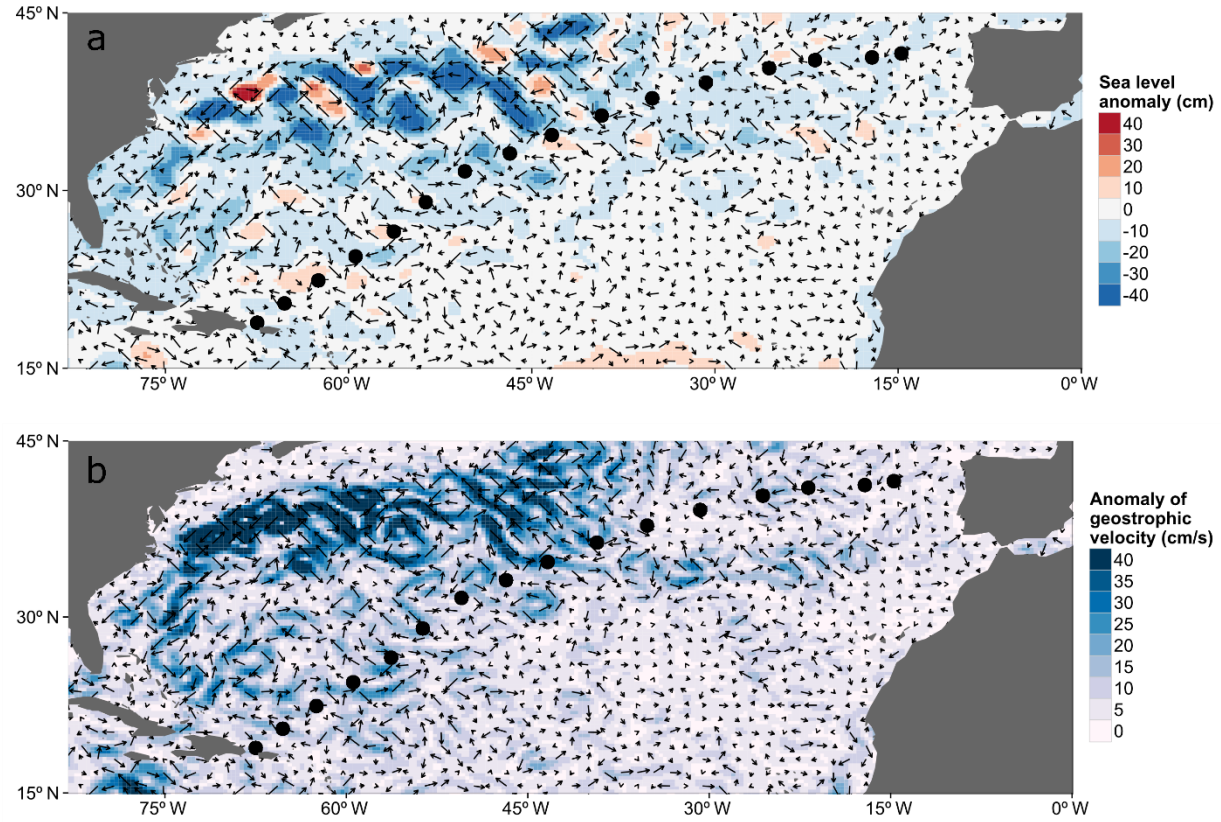

Fig 2. Satellite images showing average sea level anomalies (a) and geostrophic velocities (b) during the cruise. Black dots show the location of the stations. Scale colors indicate the magnitude of the sea level anomaly or geostrophic velocity. Arrows indicate directions of the flow.

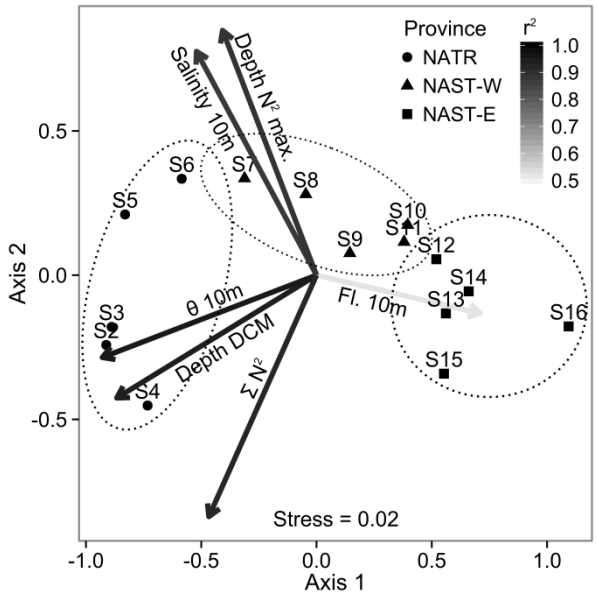

1099

1100 Fig. 3 Biplot showing the ordination of all stations retrieved from the NMDS, the directions of
1101 maximum correlation between the covariates used in the NMDS and the axes, and the
1102 classification of the stations. Stations are showed as points and variables included in NMDS are
1103 displayed as arrows. The symbols indicate the province or sub-province. Arrows point out the
1104 direction of maximum correlation between variables and the axes. Arrow heads indicate
1105 normalized linear regression coefficients between each variable and the axes (see methods).
1106 Arrow color shows values of R^2. Stress, a measure of goodness of fit, is indicated.

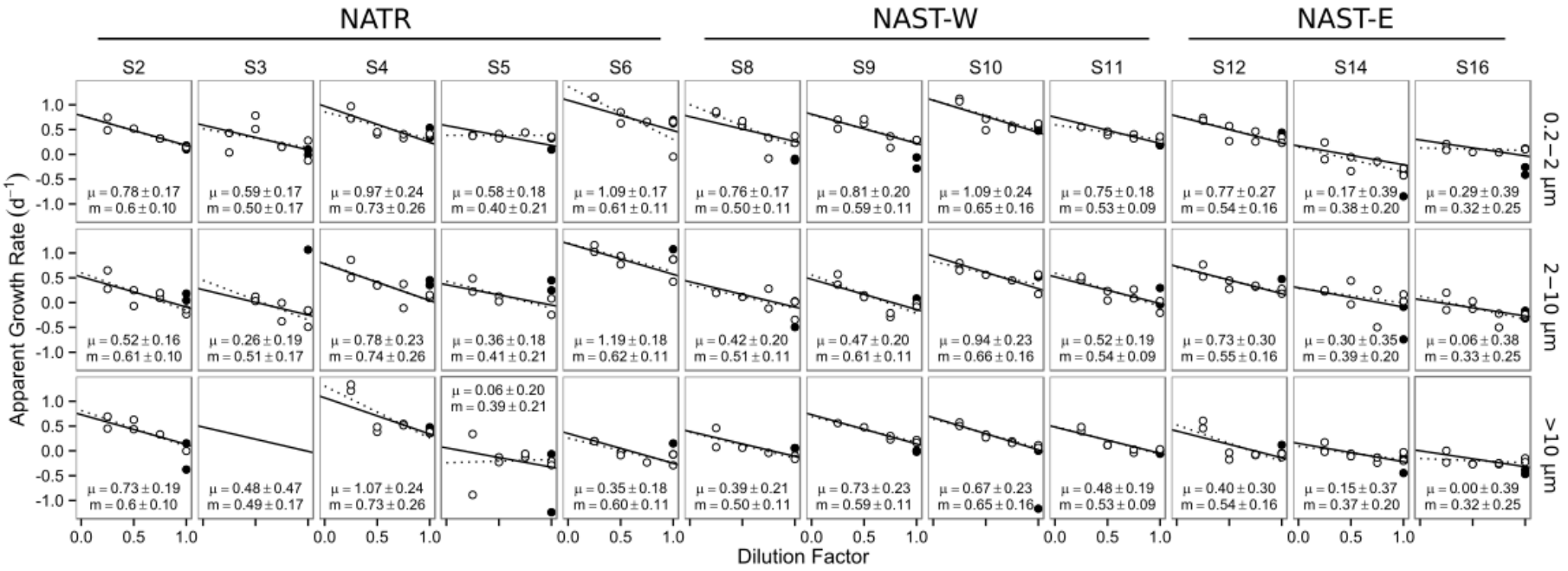

Fig. 4 Plots of dilution experiments from Chl *a* data for the different phytoplankton size fractions analyzed. White dots point out phytoplankton apparent growth rate (*r*) in treatments without nutrient addition. Black dots indicate apparent growth rate in treatments with added nutrients. Black solid lines show the fitting obtained from mixed models and model averaging. Black dotted lines show the fitting obtained from simple linear regression models for every station and size fraction. μ: phytoplankton growth rate ± 95 % confidence interval (CI) obtained from mixed models and model averaging. *m*: microzooplankton grazing rate ± 95 % CI obtained from mixed models and model averaging. Because of the low Chl *a* concentration there are not data for the size fraction > 10 µm in S3, although the use of mixed models allowed us estimating the parameters.

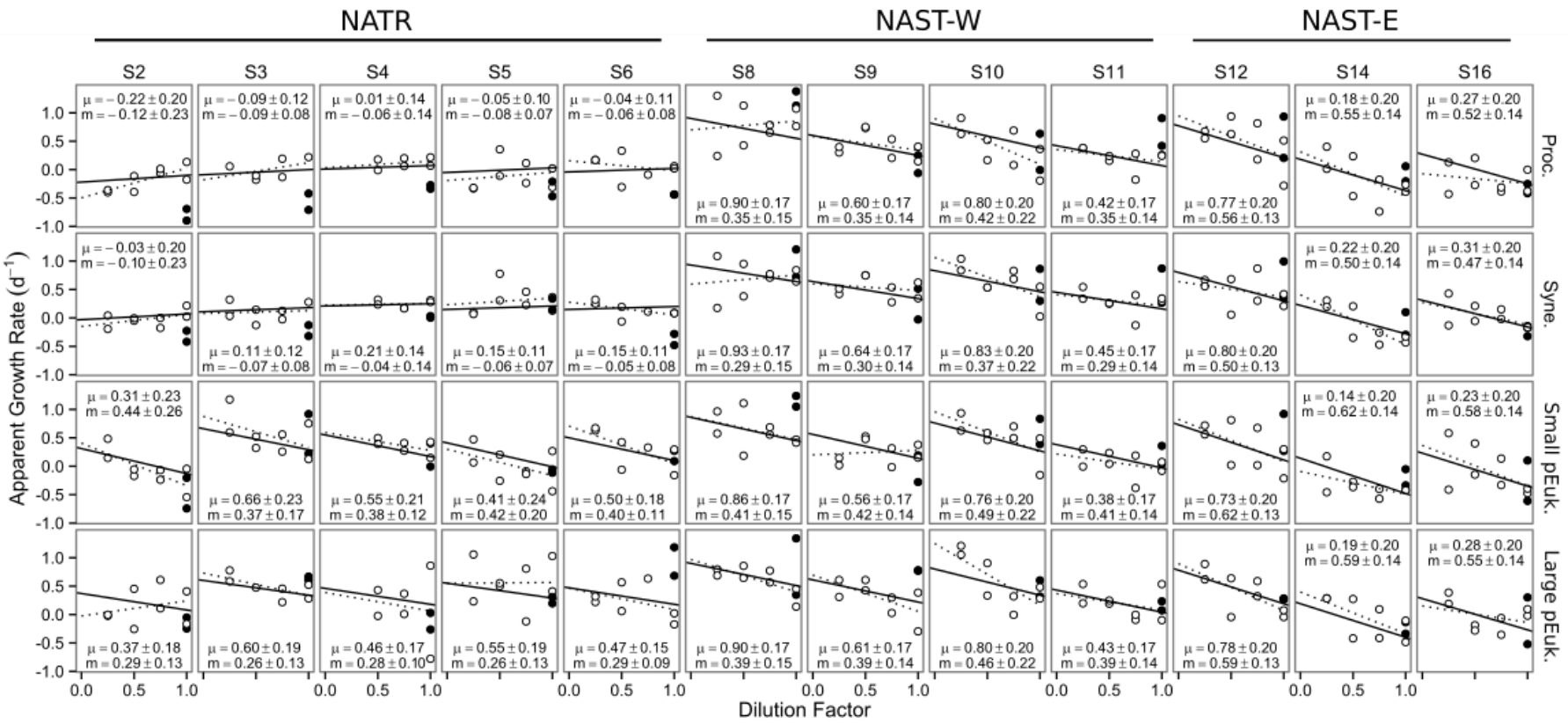

Fig. 5 Plots of dilution experiments from flow cytometry data for the different picophytoplankton groups analyzed. White dots point out phytoplankton apparent growth rate (*r*) in treatments without nutrient addition. Black dots indicate apparent growth rate in treatments with added nutrients. Black solid lines show the fitting obtained from mixed models and model averaging. Black dotted lines show the fitting obtained from simple linear regression models for every station and size fraction. μ: phytoplankton growth rate ± 95 % confidence interval

(CI) obtained from mixed models and model averaging. *m*: microzooplankton grazing rate ± 95 % CI obtained from mixed models and model averaging.

Table 3. 95 % Confidence set of models fitted with data of Chl *a* from dilution experiments. Models are ranked by AICc w. A cross (x) in *Dilution* column means that dilution factor was included in the model. Fixed and random effect columns show the different fixed and random factors included in models. The letter *I* means that an intercept (phytoplankton growth rate) was estimated for every level of the factor. The letter *S* means that a slope (microzooplankton grazing rate) was estimated in each level of the factor. K: number of parameters. AICc w scaled random str: scaled AICc w to obtain ∑ AICc w = 1 considering models with different random structures and the most complex fixed structure included in the 95 % confidence set of models. AICc w Fixed str: AICc w of models with different fixed structures conditioned on some of the better random structures. AICc w Model: AICc w obtained multiplying scaled AICc w of random structures by AICc w of fixed structures. AICc w scaled Model: scaled Model AICc w to obtain ∑ AICc w = 1. ∑ AICc w Model: Cumulative Model AICc w. ∑ AICc w scaled. Model: cumulative model AICc w using scaled model AICc w.

Rank	Fixed effects				Random effects		K	AICc w				∑ AICc w	
	Dilution	Size	Prov.	Size:Prov.	Station	Station x Size		scaled random str.	Fixed str.	Model	scaled Model	Model	scaled Model
1	x	I			S	I	15	0.6885	0.3933	0.2708	0.2838	0.2708	0.2838
2	x	I	I		S	I	17	0.6885	0.1913	0.1317	0.1381	0.4025	0.4218
3	x	I	I & S			I	15	0.3115	0.3801	0.1184	0.1241	0.5209	0.5459
4	x	I	I & S		S	I	19	0.6885	0.1219	0.0839	0.0879	0.6048	0.6339
5	x	I	I			I	13	0.3115	0.2459	0.0766	0.0803	0.6814	0.7141
6	x	I & S			S	I	17	0.6885	0.0708	0.0488	0.0511	0.7301	0.7652
7	x	I	S		S	I	17	0.6885	0.0543	0.0374	0.0392	0.7675	0.8044
8	x	I	I	I	S	I	21	0.6885	0.0463	0.0319	0.0334	0.7994	0.8379
9	x	I				I	11	0.3115	0.0821	0.0256	0.0268	0.8250	0.8647
10	x	I & S	I		S	I	19	0.6885	0.0328	0.0226	0.0237	0.8476	0.8883
11	x	I & S	I & S			I	17	0.3115	0.0655	0.0204	0.0214	0.8680	0.9097

12	x	I	I & S	I		I	19	0.3115	0.0497	0.0155	0.0162	0.8835	0.9259
13	x	I & S	I & S		S	I	21	0.6885	0.0201	0.0139	0.0145	0.8973	0.9405
14	x	I & S	I			I	15	0.3115	0.0444	0.0138	0.0145	0.9112	0.9550
15	x	I	I	I		I	17	0.3115	0.0338	0.0105	0.0110	0.9217	0.9660
16	x	I	I & S	I	S	I	23	0.6885	0.0131	0.0090	0.0095	0.9307	0.9755
17	x	I	S			I	13	0.3115	0.0273	0.0085	0.0089	0.9392	0.9844
18	x	S			S	I	15	0.6885	0.0123	0.0085	0.0089	0.9477	0.9932
19	x	I	S		S	I	19	0.6885	0.0094	0.0065	0.0068	0.9541	1.0000

Table 4. 95 % confidence set of models fitted with flow cytometry data from dilution experiments carried out in NAST. Models are ranked by AICc w. A cross (x) in *Dilution* column means that dilution factor was included in the model. Fixed and random effect columns show the different fixed and random factors included in models. The letter *I* means that an intercept (phytoplankton growth rate) was estimated for every level of the factor. The letter *S* means that the interaction with dilution factor (microzooplankton grazing rate) was estimated in each level of the factor. K: number of parameters estimated by the model. AICc w scaled random str: scaled AICc w to obtain ∑ AICc w = 1 considering models with different random structures and the most complex fixed structure included in the 95 % confidence set of models. AICc w Fixed str: AICc w of models fitted with different fixed structures and some of the better random structures. AICc w Model: AICc w obtained multiplying scaled AICc w of random structures by AICc w of fixed structures. AICc w scaled Model: scaled Model AICc w to obtain ∑ AICc w = 1. ∑ AICc w Model: Cumulative Model AICc w. ∑ AICc w scaled Model: cumulative model AICc w using scaled model AICc w.

Rank	Fixed effects				Random effects		K	AICc w				∑ AICc w	
	Dilution	Group	Prov.	Group x Prov.	Station	Station x Prov.		scaled random str.	Fixed str.	Model	scaled Model	Model	scaled Model
1	x	S	S		I		8	0.6778	0.1703	0.1154	0.1214	0.1154	0.1214
2	x	I	S		I		8	0.6778	0.1516	0.1028	0.1080	0.2182	0.2294
3	x	S	I & S		I		9	0.6778	0.1313	0.0890	0.0936	0.3072	0.3230
4	x	I	I & S		I		9	0.6778	0.1169	0.0792	0.0833	0.3864	0.4063
5	x	S	I		I		8	0.6778	0.0958	0.0649	0.0683	0.4513	0.4746
6	x	I	I		I		8	0.6778	0.0854	0.0579	0.0609	0.5093	0.5355
7	x	S	S		I & S		10	0.2457	0.1494	0.0367	0.0386	0.5460	0.5740
8	x	S	I		I & S		10	0.2457	0.1380	0.0339	0.0356	0.5798	0.6097
9	x	I	S		I & S		10	0.2457	0.1326	0.0326	0.0342	0.6124	0.6439

10	x	I	I		I & S		10	0.2457	0.1225	0.0301	0.0316	0.6425	0.6756
11	x	S			I		7	0.6778	0.0414	0.0281	0.0295	0.6706	0.7051
12	x	I			I		7	0.6778	0.0369	0.0250	0.0263	0.6956	0.7314
13	x	S	I & S		I & S		11	0.2457	0.0936	0.0230	0.0242	0.7186	0.7556
14	x	I	I & S		I & S		11	0.2457	0.0831	0.0204	0.0215	0.7390	0.7770
15	x	I & S	S		I		11	0.6778	0.0269	0.0182	0.0192	0.7573	0.7962
16	x	S			I & S		9	0.2457	0.0635	0.0156	0.0164	0.7729	0.8126
17	x	I			I & S		9	0.2457	0.0564	0.0139	0.0146	0.7867	0.8272
18	x	I & S	I & S		I		12	0.6778	0.0201	0.0137	0.0144	0.8004	0.8416
19	x	S	S			I	10	0.0765	0.1747	0.0134	0.0141	0.8137	0.8556
20	x		S		I		5	0.6778	0.0197	0.0133	0.0140	0.8271	0.8696
21	x	I	S			I	10	0.0765	0.1556	0.0119	0.0125	0.8390	0.8822
22	x	S	S	S	I		11	0.6778	0.0172	0.0117	0.0123	0.8507	0.8944
23	x		I & S		I		6	0.6778	0.0155	0.0105	0.0111	0.8612	0.9055
24	x	I & S	I		I		11	0.6778	0.0149	0.0101	0.0106	0.8713	0.9161
25	x	S	I & S			I	11	0.0765	0.1207	0.0092	0.0097	0.8805	0.9258
26	x	S	I & S	S	I		12	0.6778	0.0129	0.0087	0.0092	0.8893	0.9350
27	x	I	I & S			I	11	0.0765	0.1075	0.0082	0.0086	0.8975	0.9437
28	x		I		I		5	0.6778	0.0118	0.0080	0.0084	0.9054	0.9521
29	x	S	I			I	10	0.0765	0.0899	0.0069	0.0072	0.9123	0.9593
30	x	I	I			I	10	0.0765	0.0802	0.0061	0.0065	0.9185	0.9657
31	x	I & S	S		I & S		13	0.2457	0.0231	0.0057	0.0060	0.9241	0.9717
32	x	I & S	I		I & S		13	0.2457	0.0213	0.0052	0.0055	0.9294	0.9772
33	x	I	I & S	I	I		12	0.6778	0.0076	0.0051	0.0054	0.9345	0.9826
34	x	I & S			I		10	0.6778	0.0066	0.0045	0.0047	0.9390	0.9873
35	x	S				I	9	0.0765	0.0562	0.0043	0.0045	0.9433	0.9918
36	x		S		I & S		7	0.2457	0.0159	0.0039	0.0041	0.9472	0.9960
37	x	I	I	I	I		11	0.6778	0.0057	0.0038	0.0040	0.9511	1.0000

Table 5. 95 % confidence set of models fitted with flow cytometry data of cyanobacteria from dilution experiments carried out in NATR. Models are ranked by AICc w. A cross (x) in *Dilution* column means that dilution factor was included in the model. Fixed and random effect columns indicate the different fixed and random factors included in models. The letter *I* means that an intercept (phytoplankton growth rate) was estimated for every level of the factor. The letter *S* means that the interaction with dilution factor (microzooplankton grazing rate) was estimated in each level of the factor. K: number of parameters estimated by the model. AICc w scaled random str: scaled AICc w to obtain ∑ AICc w = 1 using models with different random structures and the most complex fixed structure included in the 95% confidence set of models. AICc w Fixed str: AICc w of models with different fixed structures and some of the better random structures. AICc w Model: AICc w obtained multiplying scaled AICc w of random structures by AICc w of fixed structures. AICc w scaled Model: scaled Model AICc w to obtain ∑ AICc w = 1. ∑ AICc w Model: Cumulative Model AICc w. ∑ AICc w scaled Model: cumulative model AICc w using scaled model AICc w.

Rank	Fixed effects		Random effects		K	AICc w				∑ AICc w	
	Dilution	Group	Station	Station x Group		scaled random str.	Fixed str.	Model	scaled Model	Model	scaled Model
1		I	I		4	0.6159	0.4046	0.2491	0.2590	0.2491	0.2590
2	x	I	I		5	0.6159	0.3887	0.2394	0.2488	0.4885	0.5077
3		I	I & S		6	0.1976	0.5764	0.1139	0.1184	0.6024	0.6261
4	x	I & S	I		6	0.6159	0.1792	0.1104	0.1147	0.7128	0.7409
5	x	I	I & S		7	0.1976	0.2823	0.0558	0.0580	0.7686	0.7989
6		I		I	6	0.1093	0.3586	0.0392	0.0407	0.8078	0.8396
7	x	I		I	7	0.1093	0.3311	0.0362	0.0376	0.8440	0.8772
8		I	S		4	0.0772	0.4025	0.0311	0.0323	0.8751	0.9095
9	x	I	S		5	0.0772	0.3892	0.0300	0.0312	0.9051	0.9407

10	x	I & S	I & S		8	0.1976	0.1239	0.0245	0.0255	0.9296	0.9662
11	x	S	I		5	0.6159	0.0268	0.0165	0.0171	0.9461	0.9833
12	x	I & S		I	8	0.1093	0.1466	0.0160	0.0167	0.9621	1.0000

1155

1156

Table 6. 95 % confidence set of models fitted with Flow cytometry data of eukaryotes from dilution experiments carried out in NATR. Models are ranked by AICc w. A cross (x) in *Dilution* column means that dilution factor was included in the model. Fixed and random effect columns show the different fixed and random factors included in models. The letter *I* means that an intercept (phytoplankton growth rate) was estimated for every level of the factor. The letter *S* means that the interaction with dilution factor (microzooplankton grazing rate) was estimated in each level of the factor. K: number of parameters estimated by the model. AICc w scaled random str: scaled AICc w to obtain ∑ AICc w = 1 using models with different random structures and the most complex fixed structure included in the 95 % confidence set of models. AICc w Fixed str: AICc w of models fitted with different fixed structures and some of the better random structures. AICc w Model: AICc w obtained multiplying scaled AICc w of random structures by AICc w of fixed structures. AICc w scaled Model: scaled Model AICc w to obtain ∑ AICc w = 1. ∑ AICc w Model: Cumulative Model AICc w. ∑ AICc w scaled Model: cumulative model AICc w using scaled model AICc w.

Rank	Fixed effects		Random effects		K	AICc w				∑ AICc w	
	Dilution	Group	Station	Station x Group		scaled random str.	Fixed str.	Model	scaled Model	Model	scaled Model
1	x			I	6	0.4384	0.3627	0.1590	0.1660	0.1590	0.1660
2	x	S		I	7	0.4384	0.3214	0.1409	0.1471	0.2999	0.3131
3	x	S	I		5	0.3573	0.3505	0.1252	0.1307	0.4252	0.4438
4	x		I		4	0.3573	0.2572	0.0919	0.0959	0.5170	0.5397
5	x	I	I		5	0.3573	0.1939	0.0693	0.0723	0.5863	0.6120
6	x	I		I	7	0.4384	0.1368	0.0600	0.0626	0.6463	0.6746
7	x	I & S		I	8	0.4384	0.1288	0.0565	0.0590	0.7027	0.7335
8	x	I & S	I		6	0.3573	0.1300	0.0464	0.0485	0.7492	0.7820
9	x			S	6	0.0850	0.4088	0.0347	0.0363	0.7839	0.8183

10	x	S	S		5	0.0851	0.3139	0.0267	0.0279	0.8107	0.8461
11	x		S		4	0.0851	0.2592	0.0221	0.0230	0.8327	0.8692
12	x	S		S	7	0.0850	0.1908	0.0162	0.0169	0.8489	0.8861
13				I	5	0.4384	0.0362	0.0159	0.0166	0.8648	0.9027
14	x	I	S		5	0.0851	0.1793	0.0153	0.0159	0.8801	0.9186
15			I		3	0.3573	0.0401	0.0143	0.0150	0.8944	0.9335
16				S	5	0.0850	0.1535	0.0130	0.0136	0.9074	0.9472
17	x	S	I & S		7	0.0342	0.3292	0.0113	0.0118	0.9187	0.9589
18	x	I		S	7	0.0850	0.1240	0.0105	0.0110	0.9292	0.9699
19		I	I		4	0.3573	0.0283	0.0101	0.0106	0.9393	0.9805
20	x	I & S	S		6	0.0851	0.1169	0.0100	0.0104	0.9493	0.9909
21	x		I & S		6	0.0342	0.2561	0.0088	0.0091	0.9581	1.0000

1167

1168

Table 7. Phytoplankton growth and microzooplankton grazing rates for every station and size fraction estimated by fitting mixed models and conducting model averaging (lmm + ma) or by fitting separate linear regression models for each experiment (lm). The 95% confidence intervals (±) are also indicated.

			NATR					NAST-W				NAST-E		
			S2	S3	S4	S5	S6	S8	S9	S10	S11	S12	S14	S16
Growth rate (d^{-1})	0.2-2 µm	lmm + ma	0.78 ± 0.17	0.59 ± 0.17	0.97 ± 0.24	0.58 ± 0.18	1.09 ± 0.17	0.76 ± 0.17	0.81 ± 0.20	1.09 ± 0.24	0.75 ± 0.18	0.77 ± 0.27	0.17 ± 0.39	0.29 ± 0.39
		lm	0.79 ± 0.25	0.52 ± 0.61	0.86 ± 0.33	0.38 ± 0.12	1.37 ± 0.55	1.01 ± 0.45	0.80 ± 0.32	1.09 ± 0.38	0.59 ± 0.14	0.78 ± 0.28	0.15 ± 0.37	0.13± 0.17
	2-10 µm	lmm + ma	0.52 ± 0.16	0.26 ± 0.19	0.78 ± 0.23	0.36 ± 0.18	1.19 ± 0.18	0.42 ± 0.20	0.47 ± 0.20	0.94 ± 0.23	0.52 ± 0.19	0.73 ± 0.30	0.30 ± 0.35	0.06 ± 0.38
		lm	0.60 ± 0.38	0.45 ± 0.80	0.80 ± 0.42	0.43 ± 0.41	1.20 ± 0.44	0.36 ± 0.65	0.56 ± 0.40	0.83 ± 0.38	0.60 ± 0.29	0.71 ± 0.24	0.29 ± 0.62	0.13 ± 0.36
	> 10 µm	lmm + ma	0.73 ± 0.19	0.48 ± 0.47	1.07 ± 0.24	0.06 ± 0.20	0.35 ± 0.18	0.39 ± 0.21	0.73 ± 0.23	0.67 ± 0.23	0.48 ± 0.19	0.40 ± 0.30	0.15 ± 0.37	0.00 ± 0.39
		lm	0.81 ± 0.36	-	1.31 ± 0.54	-0.24 ± 0.77	0.26 ± 0.25	0.38 ± 0.36	0.69 ± 0.16	0.64 ± 0.12	0.49 ± 0.22	0.52 ± 0.45	0.09 ± 0.23	-0.15 ± 0.21
Grazing rate (d^{-1})	0.2-2 µm	lmm + ma	0.60 ± 0.10	0.50 ± 0.17	0.73 ± 0.26	0.40 ± 0.21	0.61 ± 0.11	0.50 ± 0.11	0.59 ± 0.11	0.65 ± 0.16	0.53 ± 0.09	0.54 ± 0.16	0.38 ± 0.20	0.32 ± 0.25
		lm	0.63 ± 0.39	0.38 ± 0.89	0.55 ± 0.48	0.00 ± 0.20	1.07 ± 0.82	0.85 ± 0.66	0.56 ± 0.46	0.61 ± 0.56	0.30 ± 0.19	0.53 ± 0.41	0.50 ± 0.55	0.05 ± 0.24
	2-10 µm	lmm + ma	0.61 ± 0.10	0.51 ± 0.17	0.74 ± 0.26	0.41 ± 0.21	0.62 ± 0.11	0.51 ± 0.11	0.61 ± 0.11	0.66 ± 0.16	0.54 ± 0.09	0.55 ± 0.16	0.39 ± 0.20	0.33 ± 0.25
		lm	0.76 ± 0.56	0.80 ± 1.03	0.76 ± 0.62	0.54 ± 0.62	0.57 ± 0.66	0.47 ± 0.86	0.78 ± 0.58	0.47 ± 0.55	0.67 ± 0.43	0.51 ± 0.35	0.30 ± 0.90	0.47 ± 0.52
	> 10 µm	lmm + ma	0.60 ± 0.10	0.49 ± 0.17	0.73 ± 0.26	0.39 ± 0.21	0.60 ± 0.11	0.50 ± 0.11	0.59 ± 0.11	0.65 ± 0.16	0.53 ± 0.09	0.54 ± 0.16	0.37 ± 0.20	0.32 ± 0.25
		lm	0.72 ± 0.60	-	1.05 ± 0.79	-0.07 ± 1.13	0.50 ± 0.37	0.52 ± 0.52	0.52 ± 0.21	0.59 ± 0.17	0.56 ± 0.33	0.74 ± 0.66	0.27 ± 0.33	0.08 ± 0.30

Table 8. Mean phytoplankton growth and microzooplankton grazing rates for every province and size fraction estimated by fitting mixed models and conducting model averaging (lmm + ma) or by averaging the rates obtained by fitting separate linear regression models for each experiment (lm). In the latter case, we assigned a value equal to 0 to the negative rates estimated at some stations. Standard deviations (±) are also indicated.

			NATR	NAST-W	NAST-E
Growth rate (d^{-1})	0.2-2 µm	lmm + ma	0.76 ± 0.25	0.79 ± 0.26	0.56 ± 0.29
		lm	0.78 ± 0.38	0.87 ± 0.22	0.35 ± 0.37
	2-10 µm	lmm + ma	0.58 ± 0.31	0.71 ± 0.32	0.40 ± 0.34
		lm	0.70 ± 0.32	0.59 ± 0.19	0.38 ± 0.30
	> 10 µm	lmm + ma	0.50 ± 0.30	0.53 ± 0.30	0.31 ± 0.33
		lm	0.60 ± 0.58	0.55 ± 0.14	0.20 ± 0.28
Grazing rate (d^{-1})	0.2-2 µm	lmm + ma	0.54 ± 0.14	0.55 ± 0.14	0.48 ± 0.16
		lm	0.53 ± 0.39	0.58 ± 0.23	0.36 ± 0.27
	2-10 µm	lmm + ma	0.55 ± 0.14	0.56 ± 0.14	0.49 ± 0.16
		lm	0.69 ± 0.12	0.60 ± 0.15	0.43 ± 0.11
	> 10 µm	lmm + ma	0.54 ± 0.14	0.55 ± 0.14	0.48 ± 0.16
		lm	0.57 ± 0.44	0.55 ± 0.03	0.36 ± 0.34

1180 Table 9. Phytoplankton abundances (cells mL^{-1}) observed at the different stations.

Station	S2	S3	S4	S5	S6	S8	S9	S10	S11	S12	S14	S16
Cyanobacteria												
Prochlorococcus spp.	17414	21229	31088	19953	29530	10091	10111	2293	79636	6865	17718	431
Rhizomonas setigera[1]	-	-	-	-	0.04	-	-	-	-	-	-	0.04
Synechococcus spp.	4327	5458	9429	5748	12170	35833	16432	17028	39360	23520	20448	2888
Diatoms												
Chaetoceros atlanticus	-	-	-	-	-	-	-	-	-	-	-	0.92
Chaetoceros lorenz	-	-	-	-	-	-	-	-	-	-	-	0.32
Chaetoceros peruvianum	-	-	-	-	-	-	0.04	-	-	-	0.88	0.6
Corethron criophillum	-	-	-	-	-	-	-	0.04	-	0.36	0.04	2.2
Coscinodiscus spp.	-	0.04	-	-	-	-	-	-	-	-	-	-
Dactyliosolen fragilissimus	-	-	-	-	-	-	0.04	-	-	-	-	-
Guinardia striata	-	-	-	-	-	-	-	-	-	-	-	1.28
Hemiaulus spp.	-	0.04	-	0.12	-	-	-	-	-	-	-	-
Navicula spp.	0.12	-	-	-	-	-	-	0.08	0.56	0.04	0.6	3.28
Nitzschia spp.	-	0.32	0.12	0.12	0.04	0.08	1.12	-	0.96	0.48	3.92	-
Nitzschia delicatissima	-	-	-	-	-	-	-	0.6	-	-	-	268
Nitzschia longissima	-	-	-	-	-	-	-	-	0.08	-	-	-
Pleurosigma spp.	-	-	-	-	-	-	-	-	-	-	0.12	0.28
Proboscia alata	-	-	-	-	-	-	-	-	0.04	-	-	-
Rhizosolenia hebetata	-	0.04	-	-	0.04	0.04	0.04	-	0.08	-	-	-
Rhizosolenia imbricata	-	-	-	-	-	-	-	-	-	-	-	0.12
Thalassionema nitzschioides	-	-	-	-	-	-	-	-	-	-	-	0.6
Dinoflagellates												
Amphidinium spp.	0.16	-	-	-	-	0.04	-	-	-	-	-	0.04
Amphidoma caudata	-	-	-	-	-	-	-	-	-	-	-	0.04
Ceratium spp.	-	-	0.04	-	-	-	-	-	-	-	-	-
Dinophysis schuettii	-	0.04	-	-	-	-	-	-	-	-	-	-
Gymnodinium spp.	1.2	1.08	1.52	2.24	0.88	1.28	2.88	1.68	2.68	1.68	1.12	2.28
Gyrodinium spp.	-	-	0.16	0.04	0.24	0.32	0.2	0.16	0.32	0.16	0.16	1.88
Gyrodinium spirale	0.12	0.04	-	-	-	-	-	-	-	0.04	0.04	-
Heterocapsa niei	-	-	-	-	-	-	-	-	-	-	-	0.08
Katodinium glaucum	0.04	0.04	0.08	0.16	0.16	-	-	0.04	0.2	0.08	0.08	0.04
Oxytoxum scolopax	-	-	-	-	-	0.04	0.04	0.04	0.04	-	-	-
Podolampas palmipes	-	0.04	-	-	-	-	-	-	-	-	-	-
prorocentrum spp.	0.12	-	0.08	-	-	-	-	-	-	0.04	0.04	-
Prorocentrum compresum	-	-	-	-	-	-	-	-	-	-	-	0.44
Protopteridinium steinii	-	-	-	-	-	-	-	-	-	0.04	-	-
Scrippsiella trochoidea	0.16	0.12	0.12	0.08	0.12	0.12	-	0.04	0.04	-	-	-
Torodinium robustum	0.04	-	-	0.08	0.04	-	0.08	-	-	-	-	-
Torodinium spp.	-	-	0.04	-	-	0.04	-	-	-	0.08	-	-

Silicoflagellates												
Dictyocha fibula	-	0.04	-	-	-	-	0.04	0.04	-	-	0.04	1.68
Non taxonomic groups												
Large Eukaryotes	115	91	155	75	175	524	577	433	815	918	997	1188
Small Eukaryotes	320	152	128	312	325	2872	7257	15205	10424	19183	1445	621

[1] *Rhizomonas setigera* abundances are expressed in colonies mL^{-1}.

Table 10. Slopes for each province and size fraction for the relationships between size fractionated centered Chl *a* and both size fractionated phytoplankton growth rate and size fractionated microzooplankton grazing rate.

Province	Size fraction (μm)	Slope growth	Slope grazing
NATR	0.2-2	18.41	13.01
NATR	2-10	13.62	11.56
NATR	> 10	14.17	11.81
NAST-W	0.2-2	-1.32	0.28
NAST-W	2-10	-6.12	-1.17
NAST-W	> 10	-5.57	-0.92
NAST-E	0.2-2	3.55	0.94
NAST-E	2-10	-1.24	-0.51
NAST-E	> 10	-0.69	-0.26

References

Mazerolle M.J., 2013. AICcmodavg: Model selection and multimodel inference based on (Q)AIC(c). R package version 1.33. http://CRAN.Rproject.org/package=AICcmodavg.

van de Pol M. and Wright J., 2009. A simple method for distinguishing within-versus between-subject effects using mixed models. Anim. Behav. 77, 753–758.

Worden A.Z. and Binder B.J., 2003. Application of dilution experiments for measuring growth and mortality rates among *Prochlorococcus* and *Synechococcus* populations in oligotrophic environments. Aquat. Microb. Ecol. 30, 159–174.

Zuur A.F., Ieno E.N., Walker N.J., Saveliev A.A. and Smith G.M., 2009. Mixed effects models and extensions in ecology with R. Springer.